# Ginsenoside Rg3 modulates glucose metabolism and ameliorates myocardial insulin resistance through activation of AMPK pathway in TAC-induced heart failure

**Jingyu Ni**
First Teaching Hospital of Tianjin University of Traditional Chinese Medicine https://orcid.org/0000-0002-7200-7557

**Zhihao Liu**
First Teaching Hospital of Tianjin University of Traditional Chinese Medicine

**Miaomiao Jiang**
Tianjin University of Traditional Chinese Medicine

**Lan Li**
First Teaching Hospital of Tianjin University of Traditional Chinese Medicine

**Jie Deng**
First Teaching Hospital of Tianjin University of Traditional Chinese Medicine

**Xiaodan Wang**
First Teaching Hospital of Tianjin University of Traditional Chinese Medicine

**Jing Su**
Tianjin University of Traditional Chinese Medicine

**Yan Zhu**
Tianjin University of Traditional Chinese Medicine

**Feng He**
Huanggang Normal University

**Jingyuan Mao**
First Teaching Hospital of Tianjin University of Traditional Chinese Medicine

**Xiumei Gao**
Tianjin University of Traditional Chinese Medicine

**Guanwei Fan** ( guanwei.fan@tjutcm.edu.cn )
Tianjin University of Traditional Chinese Medicine

**Original investigation**

**Keywords:** Glucose metabolism, Insulin resistance, Ginsenoside Rg3, AMPK, Heart failure.

**Posted Date:** September 2nd, 2020

**DOI:** https://doi.org/10.21203/rs.3.rs-54842/v1

# Ginsenoside Rg3 modulates glucose metabolism and ameliorates myocardial insulin resistance through activation of AMPK pathway in TAC-induced heart failure

Jingyu Ni[1,2], Zhihao Liu[1], Miaomiao Jiang[3], Lan Li[1], Jie Deng[1], Xiaodan Wang[1], Jing Su[3], Yan Zhu[3],Feng He[2], Jingyuan Mao[1], Xiumei Gao[3*], Guanwei Fan[1,2,3*]

[1]Tianjin Key Laboratory of Translational Research of TCM Prescription and Syndrome, First Teaching Hospital of Tianjin University of Traditional Chinese Medicine，Tianjin 300193, China

[2] Hubei Key Laboratory of Economic Forest Germplasm Improvement and Resources Comprehensive Utilization, Huanggang Normal University, Huanggang, 438000, China

[3]Tianjin State Key Laboratory of Component-based Chinese Medicine， Tianjin University of Traditional Chinese Medicine, Tianjin 301617, China

*** Correspondence:**

**Guanwei Fan:**guanwei.fan@tjutcm.edu.cn

**Xiumei Gao:**gaoxiumei@tjutcm.edu.cn

## Abstract

**Background:** There is a close relationship between heart failure and insulin resistance, it is of great significance to carry out research on prevention and treatment of heart failure based on insulin resistance. Ginsenoside Rg3 is one of the main active ingredients in ginseng. Here, we confirmed its protective effect on the heart function of TAC-induced heart failure mice and aimed to explore the potential molecular mechanisms involved.

**Methods:** The effects of ginsenoside Rg3 on heart function and mitochondrial function were investigated by treating TAC-induced heart failure in mice. The mechanism of ginsenoside Rg3 to improve heart function and mitochondrial function in mice with heart failure was predicted through integrative analysis of proteome and plasma metabolome. Glucose uptake and myocardial insulin sensitivity were evaluated using micro-PET. Based on the above work, this experiment clarified the effect of ginsenoside Rg3 on myocardial insulin sensitivity by combining *in vivo* animal experiments and *in vitro* cell experiments. *In vivo*, the related protein expression levels of IRS-PI3K-Akt signaling pathway were detected. *In vitro*, the IR-H9c2 cardiomyocyte model was replicated with high-concentration insulin treatment, the 2-NBDG glucose uptake and transport probe was used to detect the glucose uptake of the cells, and the Western blotting method was used to detect the phosphorylation level of AMPK.

**Results:** Treatment of TAC-induced mouse models with ginsenoside Rg3 significantly reduced myocardial hypertrophy, delayed ventricular remodeling,

improved contractile and diastolic dysfunction, and protected mitochondrial structure and function. Fusion of metabolomics, proteomics and targeted metabolomics data showed that Rg3 could regulate the glycolysis process, and it has been further confirmed that Rg3 could not only regulate glucose uptake but also improve myocardial insulin resistance by using micro-PET in a mouse model of heart failure. The molecular mechanism of ginsenoside Rg3 regulating glucose metabolism was clearly determined by exploring the interaction pathways of AMPK, insulin resistance and glucose metabolism. The results showed that the effect of ginsenoside Rg3 on the promotion of glucose uptake in IR-H9c2 cells by AMPK activation was dependent on the insulin signaling pathway.

**Conclusions:** Ginsenoside Rg3 modulates glucose metabolism and significantly ameliorates insulin resistance through activation of AMPK pathway.

**Keywords: Glucose metabolism; Insulin resistance; Ginsenoside Rg3; AMPK; Heart failure.**

## Background

Heart failure is a common and complex clinical syndrome. It is a serious stage of cardiovascular disease and the leading cause of death. It is a global public health problem that needs to be solved urgently[1-2]. In the development of heart failure, not only the ventricular remodeling but also metabolic remodeling are the causes of the decline of heart function. The concept of cardiac metabolic remodeling, changes in cardiac energy metabolism pathways caused by metabolic disorders of glucose and

lipids in cardiomyocytes, was proposed by Van Bilsen *et al*. in 2004[3-4]. The main manifestations of cardiac metabolic remodeling are changes in substrate utilization, mitochondrial dysfunction, and reduction of myocardial high-energy phosphate. Under normal circumstances, the heart produces energy mainly through the two pathways of free fatty acid oxidation and glucose oxidation. Approximately 60-70% of energy production in healthy hearts is derived from β-oxidation of fatty acids, and about 20-30% is derived from the oxidation of glucose[5-7]. Changes of the two pathways of myocardial energy metabolism occur during heart failure. Among them, the glucose metabolism has obviously changed, which is mainly manifested by the weakening of the aerobic oxidation pathway of glucose by negative feedback regulation, enhanced glycolysis and lactic acid accumulation. Therefore, optimizing glucose metabolism can delay the development of heart failure.

Insulin signal transduction pathway affects multiple metabolic pathways, the most critical of which is glucose metabolism. When insulin resistance occurs, myocardial glucose uptake and utilization are disturbed[8-10]. Epidemiological evidence[11-12] confirms the close relationship between heart failure and insulin resistance. On the one hand, insulin resistance is an independent risk factor for heart failure. On the other hand, insulin resistance is also more common in patients with heart failure, and the prognosis of patients with heart failure accompanied by insulin resistance is worse[13]. The occurrence of insulin resistance is time-phase and tissue-specific. The heart is also one of the main target organs for insulin action[14-15]. Although insulin resistance alone is not sufficient to cause heart failure, it can weaken

the heart‘s compensatory ability under stress (ischemia, pressure load, or injury). Over time, the heart muscle is damaged, morphological and functional changes occur, and the occurrence and development of heart failure are accelerated. Heart failure will in turn increase insulin resistance, leading to a vicious circle[6,16-18]. Taking insulin resistance as a new basic cause of heart failure and breaking the vicious circle of heart failure and myocardial insulin resistance will provide more new strategies and new targets for the treatment of heart failure.

As an energy receptor, AMPK can enhance glucose uptake, promote fatty acid oxidation, inhibit protein synthesis, and improve insulin resistance. It plays the role of master switch in maintaining energy metabolic balance[19-20]. At the same time, there is a complex relationship between the AMPK signaling pathway and the insulin signaling pathway at the molecular level. And AMPK has become a target for the treatment of many metabolic diseases including insulin resistance. AMPK is expected to become a new target for drugs to optimize glucose metabolism and improve myocardial insulin resistance [21-22].

Ginsenoside Rg3 is one of the main active ingredients isolated from ginseng, and is also a key component of the clinical medicine Shenyi capsule. It has a variety of pharmacological effects, including antioxidant, anti-inflammatory, anti-tumor and anti-aging[23-27]. Our previous studies revealed that Rg3-loaded Pluronic F127 micelles alleviated doxorubicin-induced oxidative stress by reversing mitochondrial dysfunction[26]. And Rg3-loaded PEG-b-PPS nanoparticles alleviated MIRI by interacting with the target protein, FoxO3a, inhibited its downstream signaling

pathways, including those for oxidative stress, inflammation and fibrosis[27]. However, the specific targets and molecular mechanisms of Rg3's treatment of heart failure remain unclear. It is unclear whether the protective effect of ginsenoside Rg3 on cardiac function is due to regulating glucose metabolism and improving myocardial insulin resistance. Therefore, we investigated the potential mechanism of ginsenoside Rg3 to improve myocardial glucose metabolism and insulin resistance *in vivo* and *in vitro*.

## Materials and methods

### TAC model preparation and drug administration

Male C57BL/6 mice (18±2g) were obtained from Beijing Vital River Laboratory Animal Technology Co., Ltd. (Beijing, China), housed individually under standard conditions with a 12-h light/dark cycle, and received standard diet and water. The experimental procedures conformed to the Directive 2010/63/EU of the European Parliament, and all animals were handled according to the guidelines of the TCM Animal Research Committee (TCM-LAEC2014005) of Tianjin University of Traditional Chinese Medicine. After one week of adaptation period, the mice were randomly divided into four groups: (1) sham group, (2)model group, (3)Rg3-20mg/kg group and (4)Rg3-10mg/kg group. The mice were anesthetized with an intraperitoneal injection of 15 mg/mL tribromoethanol (30 mg/kg), the model of heart failure was induced via TAC, as described previously[28-29]. Four weeks after surgery, ginsenoside Rg3 (Shanghai Winherb Medical Technology Co., Ltd., Shanghai, China) suspended in normal saline was administered intraperitoneally (20 mg/kg/day or 10 mg/kg/day).

Mice in Sham and Model group were administrated normal saline with an equal volume via intraperitoneal injection. Twenty mice in each group were treated for four weeks (once a day).

**Echocardiographic assessment of left ventricular function**

Left ventricular function was evaluated using a Vevo 2100 (VisualSonic, Canada) ultra-high resolution animal ultrasound imaging system, as described[26-27]. The following parameters were measured as the indicators of function: systolic interventricular septum (IVSs), diastolic interventricular septum (IVSd), systolic left ventricular posterior wall (LVPWs), diastolic left ventricular posterior wall (LVPWd), ejection fraction (EF%), fractional shortening (FS%), and left ventricular mass (LV Mass).

**Hemodynamic examination**

Four weeks after administration, hemodynamics analysis was carried out by biofunction experiment system MP100-CE (BIOPAC Systems,Inc.,Santa Barbara,CA, USA) to obtain LV maximum upstroke velocity (+dp/dtmax) and maximum decrease rate (-dp/dt min).

**Histological analysis**

Four weeks after administration, mice were euthanized, and the hearts were harvested. The heart tissues were fixed using 4% paraformaldehyde for 48h, subsequently embedded in paraffin, and sliced (4-5 μm). Histologic sections of tissues were stained with hematoxylin/eosin (H&E) and Wheat germ agglutinin (WGA). For immunofluorescence (IF) analysis, sections were incubated with a mixture of mouse

anti-goat COLIα2 or COLIIIα1 polyclonal antibody and rabbit anti-goat α-Skactin polyclonal antibody (all dilutions at 1: 250), at 4 °C for 12 h. After washing with PBS, the sections were counterstained with a mixture of FITC-labeled goat anti-mouse IgG (1:30) and Cy3-labeled goat anti-rabbit IgG (1:40) at 37 °C for 1 h. After washing with PBS, the sections were mounted with water-soluble anti-quenching DAPI. Sections were examined using a fluorescence microscope and a digital camera (Carl Zeiss, Axio Observer A1).

**Real-Time Quantitative PCR Detecting**

Total RNA was extracted from mouse heart using Trizol RNA extraction kit (Invitrogen, Carlsbad, CA, USA) and the quality and concentration of the RNA were verified by spectrophotometry with a Minispine Nucleic Acid Analyzer (Thermo, USA). cDNA was generated from 1 μg of total RNA in a 20 μL reaction volume using a PrimeScript™ RT Reagent Kit (Transgen Biotech, Beijing, China). The primer sequences (Table 1) of ANP, BNP, α-SKA and β-MHC were synthesized by Sangon Biotech Co., Ltd. (Shanghai, China). cDNA products were quantified by real-time quantitative (q) reverse transcriptase polymerase chain reaction (RT-PCR) based on SYBR green labeling with a Light Cycler 480 real-time system from Roche, Co. Ltd. (Switzerland). The $2^{-\triangle\triangle Ct}$ method was used to calculate the relative expression of genes, using GAPDH as reference gene to standardize the relative expression levels of target genes.

**SDS-PAGE and Western Blot**

Mouse heart tissues or H9c2 cells were homogenized in RIPA lysis buffer and

proteinase inhibitor cocktail (1:100; Beyotime, Haimen, China). For the isolation of nucleus and cytosol proteins, the nuclear protein isolation-translocation assay kit (Sangon Biotech Co., Ltd.) was employed according to the manufacturer's protocol. Protein concentration was determined using the BCA protein assay reagent according to the manufacturer's instructions (Thermo Scientific, Waltham, MA, USA). Protein extracts were separated by electrophoresis using 4-15% SDS polyacrylamide gel and were electro-blotted onto 0.25 μm PVDF membranes. Membranes were incubated with QuickBlock™ Western blocking solution (Beyotime, Haimen, China) for 15 min at room temperature, followed by incubation overnight with primary antibodies at 4 °C (1:1000). Blots were washed five times with Tris-buffered saline/Tween 20 (TBST) and incubated with a 1:10000 dilution of horseradish peroxidase conjugated secondary antibody for 2 h at room temperature. Blots were again washed five times with TBST and developed using an ECL chemiluminescence substrate (Beyotime, Haimen, China). Band intensities were quantified using Image-J software. Western blot analysis was performed with specific primary antibodies against IRS-1, Akt-1, AS160, PDK4, GLUT4, GLUT1, GAPDH (all from Proteintech, China), AMPK, p-AMPK (both from Thermo Scientific, USA), and total OXPHOS (from Abcam, UK). The results were expressed as the relative density to GAPDH and then normalized to the mean value of the sham or control group.

**Transmission electron microscopy (TEM)**

For TEM, heart tissues were processed for ultrastructural analysis using electron microscopy[27,30]. Left ventricles were cut into three $3\times1\times1$ $mm^3$ random areas of the

cubes. Heart cubes were fixed in 2% glutaraldehyde. Then, they were osmicated in 2% OsO4, after which ultrath in sections were stained with uranyl acetate and lead citrate, and then subjected to ultrastructural examination. Pictures were taken from three random areas from three sections per mouse.

**Isolation of mitochondria**

The isolation of intact mitochondria from heart tissue was performed as previously described[31]. Tissues were used for mitochondrial isolation using mitochondrial extraction kit (Solarbio, China), and the remaining samples were quickly frozen in liquid nitrogen. Protein content of the mitochondria was quantified with BCA Protein Assay Kit (Thermo Fisher Scientific Inc, Massachusetts, USA), in accordance with the manufacturer's instructions.

**Detection of membrane potential**

TMRE and Mitotracker double staining methods were used to detect the mitochondrial inner membrane potential of isolated primary cardiomyocytes. In 2 mL of 1 μL of TMRE working solution was added, cells were stained in a 37 °C water bath for 30 minutes in the dark. Then 1 μL of Mitotracker staining solution was added to the cell suspension, and the cells were stained in a 37 °C water bath for 10 minutes in the dark. The results were observed and photographed using an inverted fluorescence microscope.

**Mitochondrial respiration**

Mitochondrial oxygen consumption rate (OCR) was assessed with a Seahorse XF24 analyzer. Mitochondria were isolated from mouse hearts as described above and

analyzed for respiration with Seahorse analyzer[32].

**Mitochondrial inner membrane permeability**

Four weeks after administration, the mouse hearts were attached to a Langendorff apparatus, with a modified Krebs–Henseleit buffer used as the perfusate (118.5mM NaCl, 25.0 mM $NaHCO_3$, 4.75 mM KCl, 1.18 mM $KH_2PO_4$, 1.27 mM $MgSO_4$, 11.0 mM d-glucose and 1.4 mM $CaCl_2$). Collagenase II-digested isolated myocardial cells were incubated in gradually increasing $Ca^{2+}$ concentrations. Cardiomyocytes were isolated and placed on laminin-coated 6-well plates coverslips for 4 h. Tetramethylrhodamine ethyl ester (TMRE) and Mitotracker double staining were performed to detect mitochondrial inner membrane permeability in isolated myocardial cells[33].

**Proteomics**

Sample was grinded in liquid nitrogen into cell powder and then transferred to a 5 mL centrifuge tube. After that, four volumes of lysis buffer (7 M urea, 1.4 M thiourea, 0.1% CHAPS) was added to the cell powder, followed by sonication three times on ice using a high intensity ultrasonic processor (Scientz). The remaining debris was removed by centrifugation at 14,000 g at 4 °C for 30 min. Finally, the supernatant was collected, and the protein concentration was determined by Bradford kit according to the manufacturer's instructions. For digestion, the protein solution was reduced with 5 mM dithiothreitol for 1 h at 60 °C and alkylated with 11 mM iodoacetamide for 10 min at room temperature in darkness. The protein sample was then diluted by adding 100 mM TEAB to urea concentration less than 2M. Finally, trypsin was added at 1:50

trypsin-to-protein mass ratio for the first digestion overnight and 1:100 trypsin-to-protein mass ratio for a second 4 h-digestion. After trypsin digestion, peptide was desalted by Strata X C18 SPE column (Phenomenex) and vacuum dried. Peptide was reconstituted in 0.5M TEAB and processed according to the manufacturer's protocol for TMT kit/iTRAQ kit. Briefly, one unit of TMT/iTRAQ reagent were thawed and reconstituted in acetonitrile. The peptide mixtures were then incubated for 2 h at room temperature and pooled, desalted and dried by vacuum centrifugation. The tryptic peptides were dissolved in 0.1% formic acid (solvent A), directly loaded onto a home-made reversed-phase analytical column (15-cm length, 75 μm i.d.). The gradient was comprised of an increase from 6% to 23% solvent B (0.1% formic acid in 98% acetonitrile) over 26 min, 23% to 35% in 8 min and climbing to 80% in 3 min then holding at 80% for the last 3 min, all at a constant flow rate of 400 nL/min on an EASY-nLC 1000 UPLC system. The peptides were subjected to NSI source followed by tandem mass spectrometry (MS/MS) in Q ExactiveTM Plus (Thermo) coupled online to the UPLC. The electrospray voltage applied was 2.0 kV. The m/z scan range was 350 to 1800 for full scan, and intact peptides were detected in the Orbitrap at a resolution of 70,000. Peptides were then selected for MS/MS using NCE setting as 28 and the fragments were detected in the Orbitrap at a resolution of 17,500. A data-dependent procedure that alternated between one MS scan followed by 20 MS/MS scans with 15.0s dynamic exclusion. Automatic gain control (AGC) was set at 5E4. Fixed first mass was set as 100 m/z. The mass spectrometry analysis of iTRAQ is completed by Thermo Q-Exactive mass

spectrometry, and the original files of mass spectrometry generated are processed by Proteome Discoverer 1.4, a supporting commercial software of Thermo.

**Metabolic Profiling**

Mouse blood was placed in a pre-heparinized centrifuge tube and placed in a 37°C water bath for 30 min. Then the blood was centrifuged at 3000 rpm for 15 min, and the plasma was divided into 1.5 mL centrifuge tubes and stored at -80 ℃. Plasma metabolism profile was analyzed based on NMR Measurements. One-dimensional hydrogen spectrum was analyzed using MestReNova 6.1.0 (MestreLabResearch S.L, Spain) software. Taking the TSP methyl proton signal as δ 0 ppm, the δ 0.6-10.0 ppm range is integrated in sections, the integration step is set to 0.01 ppm, and the residual signal of the water peak in the δ 4.71-5.14 ppm range is eliminated. The obtained NMR integral data is normalized and Pareto scaled and then imported into MetaboAnalyst 3.0 (www.metaboanalyst.ca) software for principal component analysis (PCA) and orthogonal partial least squares discriminant analysis (OPLS-DA).

**Quantitative analysis of energy metabolites in mouse heart tissue by LC-MS/ MS**

1 mL of pre-cooled methanol/acetonitrile/water (2:2:1, v/v/v) was added to the sample. After the samples were vortex mixed, the samples were sonicated for 30 min in an ice bath. The samples were then incubated at -20 °C for 1 h to precipitate proteins, centrifuged at 14000 rcf at 4 ° C for 20 min, and the supernatant was taken and dried in vacuo. For mass detection, 100 μL of acetonitrile-water solution (1:1, v/v) was added to reconstitute. After centrifugation at 14000 rcf at 4°C for 15 min, the supernatant was diluted twice and injected for analysis. The samples were separated

using the Agilent 1290 Infinity LC ultra-high performance liquid chromatography system. Mobile phase: solution A was 15 mM ammonium acetate aqueous solution, and solution B was acetonitrile. The sample was placed in a 4°C autosampler, the column temperature was 45°C, the flow rate was 300 μL/min, and the injection volume was 4 μL. The relevant liquid phase gradient was as follows: Liquid B changed linearly from 90% to 40% in 0-18 min; Liquid B changed linearly from 40% to 90% in 18-18.1 min; Liquid B was maintained at 90% in 18.1-23 min. The QC samples in the sample queue were set for testing and evaluating the stability and repeatability of the system; The standard mixture of energy metabolites in the sample cohort was used to correct the chromatographic retention time. A 5500 QTRAP mass spectrometer (AB SCIEX) was used for mass spectrometry analysis in negative ion mode. 5500 QTRAP ESI source conditions are as follows: source temperature 450°C, ion Source Gas1 (Gas1): 45, Ion Source Gas2 (Gas2): 45, Curtain gas (CUR): 30, ionSapary Voltage Floating (ISVF) -4500 V; The ion pair was detected in MRM mode. Multiquant software was used to extract chromatographic peak area and retention time. Standards of energy metabolites were used to correct retention time, and metabolites were identified.

**Glucose metabolism monitoring by 18-fluorodeoxyglucose small animal positron emission computed tomography**

In the basic state: the mice were fed normally, the oxygen flow was controlled at 400mL/min, and the tail vein bolus injection 50-70 μL 18F-FDG 200-300 uci (7.4-11.1 MBq) for micro PET dynamic imaging for 60 min under 1.5%-1.8%

isoflurane anesthesia. After image reconstruction, the myocardial region of interest (ROI) was delineated to obtain the myocardial time-radioactivity curve (TAC), and the myocardial glucose standard uptake value (SUV) was calculated.

Under insulin stimulation: the mice were fed normally, and intraperitoneal injection of insulin 10-15 U/kg was performed 30 minutes before the micro PET test, the oxygen flow was controlled at 400 mL/min, and the tail vein bolus injection 50-70 μL 18F-FDG 200-300 uci (7.4-11.1 MBq) for micro PET dynamic imaging for 60 min under 1.5%-1.8% isoflurane anesthesia. After image reconstruction, the myocardial region of interest (ROI) was delineated to obtain the myocardial time-radioactivity curve (TAC), and the myocardial glucose standard uptake value (SUV) was calculated.

**Cell viability assay**

MTT assay was used to detect the viability of the cell viability. H9C2 were seeded on 96-well plates with a density of $1\times10^5$ cells/mL in 100 μL complete medium for 12 hrs. Subsequently, the cells were incubated with various concentrations of ginsenoside Rg3 in 37℃ and 5% CO2 incubator for 24 h. 10μL MTT was added into each well and incubated for 4 hrs in the dark, and then culture medium was removed with extra addition of 150 μL DMSO to resolve the formazan. Finally, optical density (OD) of the formazan of each well was measured with a microplate reader (Molecular Devices, USA) at 570 nm.

**Glucose uptake in H9c2 cells using 2-NBDG as fluorescence probe**

H9c2 cardiomyocytes were seeded in 96-well plates with approximately $10^5$ cells per

well and incubated for 24 hours. Cells were treated with corresponding reagents or drugs for 24 h. Cells were treated with 0 or 100 μmol/L insulin for 30 min, washed twice with KRB, and then treated with 100 μmol/L 2-NBDG for 30 min at 37℃, washed twice with KRB. Changes in intracellular fluorescence intensity were measured using a fluorescence microplate reader (Ex/Em, 488/520 tim) to assess the uptake of 2-NBDG by H9c2 cardiomyocytes. Finally, the fluorescence intensity of cells in each well was corrected by MTT analysis. The experiment was repeated 3 times.

**Statistical Analysis**

Te experimental processes and experimental data analyses were carried out following randomization. The experimental data are expressed as means ±SD. GraphPad Prism 8.0 software was used for data analysis. A one-way-ANOVA followed by an LSD post hoc test were used to test the differences between groups. A $p$ value less than 0.05 was considered statistically significant.

# Results

**Ginsenoside Rg3 reduced myocardial hypertrophy and delayed ventricular remodeling**

To investigate the potential protective effects of ginsenoside Rg3 in HF, we conducted a study with a mouse model of HF induced by transverse aortic constriction (TAC). Compared with a sham group, the TAC mice displayed expanded hearts with significantly increased heart weight-to-tibia length ratio (HW/TL), left ventricular mass-to-tibia length ratio (LV mass/TL) and the systolic and diastolic left ventricular

volume (Fig. 1a-e) and upregulated expression of the ANP, BNP, β-MHC and α-SKA genes (Fig. 1f-i). To investigate the effect of ginsenoside Rg3 in TAC-induced HF, four weeks after TAC surgery, the mice were treated with either a low dose (10 mg/kg/day) or a high dose (20 mg/kg/day) of Rg3. Compared with the TAC group, both Rg3-treatment groups exhibited significant improvement of myocardial hypertrophy, with decreased HW/TL, LV mass/TL ratios, the systolic and diastolic left ventricular volume and WGA (Fig. 1a-e). The lower expression of the ANP, BNP, β-MHC and α-SKA genes provided further evidence of the protection of Rg3 in TAC-induced HF (Fig. 1f-i). From the histological assessment of heart tissues, we found reduced cell size in Rg3-treated mice (Fig. 1j-k) and the content of type I and type III collagen in the heart (Fig. 1l-m).

**Ginsenoside Rg3 improved cardiac function in mice with chronic heart failure induced by TAC**

The effects of ginsenoside Rg3 on cardiac functions were assessed by echocardiography. As shown by the M-model echocardiograms (Fig. 2a), the ventricular cavity was dilated, and the left ventricular wall motion was weakened in the model group. In comparison, the amplitude of the left ventricular wall motion was stronger after the treatment with ginsenoside Rg3. The ejection fraction (EF%) and short-axis shortening rate (FS%) in the model group were significantly lower than that of the sham group ($P < 0.01$ vs Sham). Compared with the model group, EF% and FS% were significantly increased after ginsenoside Rg3 treatment ($P < 0.01$ vs Model, Fig. 2a-c). From the histological assessment of heart tissues, we found reduced

inflammatory cell infiltration and diffuse edema in Rg3-treated mice (Fig. 2d), indicating that ginsenoside Rg3 could improve cardiac function in mice with chronic heart failure induced by TAC. The maximum increase rate (+dp/dt max) and maximum decrease rate (-dp/dt max) of the mice in the model group were decreased ($P < 0.01$ vs Sham, $P < 0.01$ vs Sham). The maximum decrease rate was not significantly improved after the administration of ginsenoside Rg3. However, administration of ginsenoside Rg3 significantly improved the maximum increase rate ($P < 0.05$, vs model, Fig. 2e-g).

**Ginsenoside Rg3 improves mitochondrial ultrastructure and function in mice with chronic heart failure induced by TAC**

The ultrastructure of mitochondria was observed through transmission electron microscope. Compared with the sham group, myocardial mitochondria in the TAC model group showed disordered arrangement, obvious edema and ablation of mitochondrial crest. After treatment with ginsenoside Rg3, the mitochondria of the myocardium were neatly arranged, the mitochondrial edema was reduced, and the mitochondrial crest was relatively clear and complete (Fig. 3a). To examine whether ginsenoside Rg3 treatment resulted in changes in mitochondrial function, the cells were loaded with tetramethylrhodamine ethyl ester (TMRE) to indicate mitochondrial inner membrane permeability in the mitochondria. Compared with the sham group, TMRE fluorescence intensities were obviously weakened in myocardial cells in the model group, whereas ginsenoside Rg3 treatment resulted in enhanced fluorescence intensity (Fig. 3b). The potential of ginsenoside Rg3 for enhancing mitochondrial

function in cardiac hypertrophy was assessed by ATP production, spare respiratory capacity and maximal mitochondrial respiration rates. The hypertrophic myocardial cells showed a significantly decline in ATP production, spare respiratory capacity and maximal mitochondrial respiration rates in comparison to the sham group (Fig. 3c-f). Ginsenoside Rg3 treatment resulted in increased ATP production ($P < 0.01$, vs model), improved spare respiratory capacity ($P < 0.05$, vs model) and enhanced maximal mitochondrial respiration rates ($P < 0.01$, vs model).

Furthermore, to confirm the effect of ginsenoside Rg3 on mitochondrial function, we detected the protein content of transport chain complexes (ETC) in isolated mitochondria from the heart tissue. As shown in Fig. 3g-l, the protein content of complexes I, II, III, and IV were no significantly changes in TAC group and Rg3 treatment group.

**Fusion of proteomics and metabolomics data showed that ginsenoside Rg3 had a moderating effect on glycolysis / gluconeogenesis**

The utilization process of substrate is one of the important links of myocardial energy metabolism pathway. During the development of heart failure, hypertrophic and failed myocardium often undergo changes in substrate metabolism, and directly or indirectly promote the development of myocardial remodeling. Therefore, on the basis of previous experiments, we took heart tissue and plasma as the research objects and predicted the mechanism of ginsenoside Rg3 protecting myocardial injury in heart failure mice through joint analysis of cardiac proteomics and plasma metabolomics.

Differential proteins were screened using Maxquant's Significance A to calculate the p

value after calculating the corresponding ratio. Fold change 1.5 times and p value <0.05 were considered significant differences. Heat map analysis (Fig. 4a-b) showed that ginsenoside Rg3-20 mg/kg had a significant effect on 16 abnormally changed proteins and ginsenoside Rg3-10 mg/kg had a significant effect on 25 abnormally changed proteins in the heart failure model. Protein information was shown in Table 2-3. The metabolite profiles of mouse plasma were collected using $^{1}$H-NMR technology. When the screening condition was VIP > 1, 275, 221, and 278 variables were extracted from the three comparisons, and 59 variables related to heart failure, which were regulated by ginsenoside Rg3, were further screened by Venn analysis. Based on the structural information given by each variable, 10 metabolites were identified (Fig. 4c) as key metabolic markers related to heart failure regulated by ginsenoside Rg3.

After that, we conducted a joint analysis of proteomics and metabolomics data, and the screening method was based on the previous literature (Cell 2016, 167, 829–842). Proteins with a fold change≥1.5 and at a P-value < 0.05 were significant differently expressed proteins. Metabolites with a fold change≥1.5 and at a P-value < 0.1 were significant differentially expressed metabolites. A total of 118 differential proteins and 18 differential metabolites were screened. Detailed analysis of enrichment pathway showed that three pathways, glycolysis/gluconeogenesis, glycerophospholipid metabolism and alanine/aspartate/glutamate metabolism were involved in both differential proteins and differential metabolites (Fig. 5a-c).

**Quantitative analysis of energy metabolites showed that ginsenoside Rg3**

**exherted significant homeostatic effect on multiple metabolites during glycolysis and tricarboxylic acid cycle**

Based on the results of the joint analysis of proteomics and metabolomics, we next examined the content of 17 important metabolites in the glycolytic pathway and the tricarboxylic acid cycle by LC-MS/MS. Using a detection process shown in Figure 6a, data were quantified according to metabolic pathways. The results showed that ginsenoside Rg3 exherted significant homeostatic effect on phosphoenolpyruvate, pyruvate, acetyl CoA, aconitic acid, isocitrate, succinic acid, fumaric acid and oxaloacetic acid (Fig. 6b).

**Ginsenoside Rg3 regulated glucose uptake and myocardial insulin sensitivity in mice with heart failure**

The above experimental results revealed an altered glucose metabolism of heart failure mice, which can be effectively restored by ginsenoside Rg3. Therefore, protein expressions of glucose transporter 4 (GLUT4) was detected to further investigate the effect of ginsenoside Rg3 on substrate utilization changes. As shown in Figure 6c-e, myocardial glucose transporter 4 (GLUT4) was significantly increased in model group compared with that of the sham group. Both high (20 mg/kg) and low (10 mg/kg) doses of ginsenoside Rg3 normalized glucose utilization. Changes in myocardial glucose metabolism in mice were monitored using 18-fluorodeoxyglucose (18-FDG) positron emission tomography (micro PET). In the basal state, compared with the sham group, the myocardial SUV of the model group was significantly increased ($P < 0.05$). In contrast, treatment with ginsenoside Rg3 (20 mg/kg)

459 significantly reduced myocardial glucose metabolism compared with the model group
460 ($P < 0.05$). These results showed that ginsenoside Rg3 had a significant regulatory
461 effect on myocardial glucose metabolism in chronic heart failure induced by TAC (Fig.
462 6f-g). However, under the condition of insulin stimulation, myocardial glucose
463 metabolism of the sham group was significantly increased after insulin stimulation.
464 Compared with the sham group, myocardial SUV in the model group did not increase
465 significantly after insulin stimulation, suggesting that the mice in the model group had
466 myocardial insulin resistance. Ginsenoside Rg3 (20 mg/kg) significantly increased the
467 myocardial glucose metabolism after insulin stimulation ($P < 0.05$), suggesting that
468 ginsenoside Rg3 could significantly improve the myocardial insulin resistance of
469 chronic heart failure induced by TAC (Fig. 6f-g). At the same time, systemic insulin
470 sensitivity was also measured, but the results showed that there was no significant
471 change in serum glucose and insulin levels between groups (Fig. S1a-b).

472 **Ginsenoside Rg3 had a regulatory effect on protein levels of myocardial insulin**
473 **signaling pathway and phosphorylation of AMPK protein**

474 Insulin resistance blocks the IRS-PI3K-Akt signaling pathway, which is associated
475 with glucose transporter (GLUT4) transport and translocation, thereby affecting
476 myocardial substrate utilization and energy metabolism. Therefore, expression levels
477 of IRS-PI3K-Akt signaling pathway-related proteins were detected. As shown in
478 Figure 6, expression of IRS1, Akt, and AS160 proteins in the myocardial
479 IRS-PI3K-Akt signaling pathway of the model group were inhibited compared with
480 those in the sham group, leading to the disorder of myocardial glucose metabolism.

Treatment with ginsenoside Rg3 (20 mg/kg) increased the expression of IRS-PI3K-Akt signaling pathway-related proteins (Fig. 6h-l). Compared with the sham group, the phosphorylated AMPK protein expression in the model group was also reduced, which were restored by the treatment with ginsenoside Rg3 at either high (20 mg/kg) or low (10 mg/kg) doses, suggesting that AMPK might be a potential target for ginsenoside Rg3 to regulate glucose metabolism.

**The effect of ginsenoside Rg3 on the promotion of glucose uptake in IR-H9c2 cells by AMPK activation was dependent on the insulin signaling pathway**

Based on the above studies, we established IR-H9c2 cardiomyocyte model with high concentration insulin treatment to investigate the effect of ginsenoside Rg3 on glucose uptake and AMPK activity. MTT results showed that there was no significant difference on cell proliferation between treatment with 0.1 μmol/L, 1 μmol/L or 10 μmol/L ginsenoside Rg3 and the control group (0 μg/mL) ($P > 0.05$). However, when the concentration of ginsenoside Rg3 reached 100 μmol/L, it had a significant inhibitory effect on the proliferation of H9c2 cardiomyocytes ($P < 0.05$, Fig. 7a). Therefore, 10 μmol/L was selected as the treatment concentration of ginsenoside Rg3 in the subsequent experiments. In normal H9c2 cells, there was no significant difference in the total AMPK protein expression of each group. However, ginsenoside Rg3 significantly increased the AMPK phosphorylation at Thr172. Compound C, a selective inhibitor of AMPK, significantly reduced the phosphorylation level of AMPK at Thr172 in H9c2 cardiomyocytes stimulated by ginsenoside Rg3 (Fig. 7b-c). In IR-H9c2 cells, the phosphorylation of AMPK at

503 Thr172 was decreased significantly in the IR group compared with the control group
504 ($P < 0.01$) whereas ginsenoside Rg3 significantly increased the phosphorylation level
505 of AMPK at Thr172 compared with IR group ($P < 0.01$). Compound C significantly
506 reduced the phosphorylation level of AMPK at Thr172 of ginsenoside Rg3 stimulated
507 IR-H9c2 cardiomyocytes (Fig. 7d-e). Next, the effect of ginsenoside Rg3 on glucose
508 uptake in IR-H9c2 cardiomyocytes was evaluated using a fluorescent probe for
509 glucose uptake 2-NBDG. Compared with the control group, the sensitivity of insulin
510 in the IR group decreased, and insulin-stimulated glucose uptake was significantly
511 reduced ($P < 0.05$), suggesting that there was insulin resistance in H9c2 cells in the IR
512 group. Compared with the IR group, ginsenoside Rg3 significantly increased
513 insulin-stimulated glucose uptake ($P < 0.05$). To confirm whether AMPK is involved
514 in glucose uptake stimulated by ginsenoside Rg3 in IR-H9c2 cardiomyocytes,
515 Compound C was used to pretreat IR-H9c2 cardiomyocytes and glucose uptake was
516 measured. We found that Compound C significantly reduced ginsenoside Rg3-
517 stimulated glucose uptake in IR-H9c2 cardiomyocytes. The results suggest that
518 ginsenoside Rg3 can promote glucose uptake of IR-H9c2 cardiomyocytes, and this
519 effect is related to the activation of AMPK (Fig. 7f). On the basis of previous
520 experiments, IRS1 gene was silenced in cardiomyocytes, and changes in glucose
521 uptake levels were observed. At the same time, the activator AICAR were used to
522 investigate whether the effect of ginsenoside Rg3 on promoting glucose uptake in
523 IR-H9c2 cells by activating AMPK is dependent on the insulin signaling pathway. The
524 results showed that the effect of ginsenoside Rg3 on the promotion of glucose uptake

525 in IR-H9c2 cells by AMPK activation was dependent on the insulin signaling
526 pathway(Fig. 7g).

527 ## Discussion

528 The substrates of cardiac energy metabolism are mainly fatty acids and glucose, and
529 the rate of heart work is closely related to the metabolic rate of energy substrates.
530 However, in the process of heart failure, hypertrophic and failed myocardium often
531 undergo changes in energy and substrate metabolism, and directly or indirectly
532 promote the development of myocardial remodeling, that is, the “metabolic
533 remodeling” of myocardial energy. Myocardial metabolic remodeling of heart failure
534 is one of the research hotspots in recent years. Metabolic dysfunction was originally
535 thought to be a myocardial defect, but it is now considered to be a complex interaction
536 process between the myocardium and surrounding tissues and organs. Effectively
537 improving metabolic remodeling has become an important link in the treatment of
538 heart failure[3-6,34-35]. Although glucose is only a secondary substrate for cardiac
539 metabolism, it produces more energy compared with fatty acid metabolism, when the
540 same unit of oxygen is consumed. In the early stages of heart failure, myocardial
541 metabolism begins to shift to glucose metabolism. In this way, the myocardium can
542 complete the tricarboxylic acid cycle with little oxygen to produce more energy. But
543 as the disease progresses, compensatory glycolysis increases, and the balance between
544 glycolysis and glucose oxidation is severely disturbed. The increased glycolysis not
545 only does not compensate for the lack of energy, but also does not match the oxidation
546 of pyruvate and lactic acid, resulting in a large accumulation of hydrogen ions and

calcium ions in the cytoplasm, resulting in further damage to heart function. Therefore, inducing and improving the glucose oxidation pathway and reducing the increased compensatory glycolysis is an important strategy for the treatment of heart failure[36-38]. In this study, since the analysis results of proteomics and metabolomics revealed that ginsenoside Rg3 could regulate the glycolysis and gluconeogenesis pathways, we performed a MRM-based quantitative analysis of the energy metabolites in mouse heart tissue. The test covered 17 important metabolites in the glycolysis pathway and the tricarboxylic acid cycle. The results showed that ginsenoside Rg3 had a significant recuperative effect on phosphoenolpyruvate, pyruvate, and acetyl CoA. Aconitic acid, isocitric acid, succinic acid, fumaric acid and oxaloacetic acid were significantly regulated during the tricarboxylic acid cycle. These results indicated that compensatory glycolysis in the myocardium of heart failure mice was increased, and the ginsenoside Rg3 could reduce the increased compensatory glycolysis, thereby achieving a balance between glycolysis and oxidation.

Since the concept of “metabolic syndrome” was introduced by Reaven in 1988, insulin resistance has been actively investigated in various fields. Insulin resistance refers the ability of insulin to promote glucose uptake and utilization of target organs /tissues is reduced, resulting in a series of pathophysiological changes. The link between insulin resistance and heart failure has been proposed for more than a century. Epidemiological evidence suggests that insulin resistance and heart failure go far beyond a simple correlation. A Swedish study in 2005 of 1187 male patients who had not previously experienced heart failure [11] confirmed that insulin resistance precedes

heart failure and not subsequently and found that insulin resistance is predictive of subsequent heart failure and is independent of all established risk factors, including diabetes itself. A 2013 American clinical study[12] explored more directly the relationship between insulin resistance and heart failure. The study included 12,606 subjects without heart failure and found that insulin resistance occurs before heart failure and is independent of other risk factors, including diabetes. This epidemiological evidence confirms the close relationship between heart failure and insulin resistance, suggesting that insulin resistance is an independent risk factor for the development of heart failure. On the other hand, patients with heart failure also have insulin resistance more commonly, and patients with heart failure associated with insulin resistance have a worse prognosis[13]. The occurrence of insulin resistance is time-phase and tissue-specific. The heart is also one of the main target organs for insulin action[14]. Clinical studies have shown that after scanning the myocardium of patients with heart failure with PET, the uptake of fluorodeoxyglucose in the myocardium under insulin stimulation was significantly reduced, indicating the presence of myocardial insulin resistance [15]. Therefore, patients with heart failure not only have systemic insulin resistance, but also often have myocardial insulin resistance. However, because the myocardium only accounts for 0.5% of the body weight, it has little effect on the overall blood glucose level, and myocardial insulin sensitivity has not attracted enough attention. More and more evidence show that myocardial insulin resistance is directly related to the occurrence and development of cardiovascular disease.

In this study, micro-PET was used to observe changes in glucose uptake and changes in glucose metabolism in the myocardium of mice under insulin stimulation were observed. The results showed that the model group had myocardial insulin resistance, and ginsenoside Rg3 could significantly improve the myocardial insulin resistance of chronic heart failure induced by TAC.

Glucose uptake is one of the rate-limiting steps of glucose metabolism. It is regulated both by the insulin signaling and AMPK signaling pathways. Recepto-binding of insulin activates the insulin receptor substrate (IRS-PI3K-Akt) signaling pathway and the Ras-MAPK signaling pathways. Recent studies have shown that when insulin resistance occurs, the blockage of the signaling pathway is often selective, that is, the IRS-PI3K-Akt signaling pathway is blocked. And the IRS-PI3K-Akt pathway is related to the translocation of glucose transporter (GLUT4) and FA translocation enzyme (CD36), which affects myocardial substrate utilization and energy metabolism[39-41]. The results of this study suggested that myocardial insulin resistance was directly related to the occurrence and development of heart failure, and ginsenoside Rg3 can affect the translocation of glucose transporter (GLUT4) and glucose uptake through the IRS-PI3K-Akt pathway, and ultimately affect myocardial glucose metabolism. As an energy regulator, AMPK has been paid more and more attention to the regulation of intracellular energy balance. Many studies have shown that AMPK signaling pathway plays an important regulatory role in glucose, fatty acid and protein metabolism. In terms of glucose metabolism, AMPK not only promotes glucose uptake and oxidation, but also directly stimulates the phosphorylation of

AS160. After AS160 was phosphorylated by Akt, its GTPase activating protein (GAP) activity was inhibited, resulting in more Rab proteins being converted into GTP-binding proteins. GLUT-4 is then promoted to translocate to the cell membrane to enhance glucose uptake. While stimulating GLUT-4 membrane translocation, AMPK activation can also phosphorylate the glycolytic rate-limiting enzyme, phosphofructokinase (PFK), thereby promoting glycolysis. In our study, the protein level of phosphorylated AMPK was detected. The results suggested that ginsenoside Rg3 could increase the content of phosphorylated AMPK protein and AMPK might be a potential target for ginsenoside Rg3 to regulate glucose metabolism. At the same time, there is a complex correlation between the AMPK signaling pathway and the insulin signaling pathway at the molecular level. As AMPK has become a target for the treatment of many metabolic diseases including insulin resistance, our data support its being a new target for the treatment of myocardial insulin resistance [19-22].

This study found that ginsenoside Rg3 increased the AMPK activity of IR-H9c2 cardiomyocytes, and Compound C, an AMPK inhibitor, significantly reduced the role of ginsenoside Rg3 in stimulating glucose uptake in IR-H9c2 cardiomyocytes. This result indicated that ginsenoside Rg3 promoted glucose uptake of IR-H9c2 cardiomyocytes at least in part by activating AMPK. Then, what role do AMPK and insulin signaling pathway play in ginsenoside Rg3-stimulated glucose uptake in IR-H9c2 cardiomyocytes? On the basis of previous experiments, IRS1 gene was silenced in cardiomyocytes, and changes in glucose uptake levels were observed. At the same time, the AMPK inhibitor Compound C and the activator AICAR were used

to investigate whether the effect of ginsenoside Rg3 on promoting glucose uptake in IR-H9c2 cells by activating AMPK is dependent on the insulin signaling pathway. The results showed that the effect of ginsenoside Rg3 on the promotion of glucose uptake in IR-H9c2 cells by AMPK activation was partially dependent on the insulin signaling pathway.

In this study, the results of proteomics and metabolomics also suggested that ginsenoside Rg3 might have a potential regulatory effect on alanine/aspartate/ glutamate metabolism and glycerophospholipid metabolism, a finding worthy of in-depth study in the future. The mechanism analysis in this study is only performed at the cellular level, and there are certain limitations. Because the cell environment is relatively simple, the mechanism should be further explored at the overall level in subsequent research.

## Conclusion

Ginsenoside Rg3 stimulates glucose metabolism and significantly ameliorates insulin resistance through activation of AMPK pathway.

## Ethics approval and consent to participate

The experimental procedures conformed to the Directive 2010/63/EU of the European Parliament, and all animals were handled according to the guidelines of the TCM Animal Research Committee (TCM-LAEC2014005) of Tianjin University of Traditional Chinese Medicine.

## Consent for publication

Not applicable.

## Availability of data and materials

All data are provided and available in this manuscript.

## Competing interests

The authors declare that they have no competing interests.


## Funding

This work was supported by grants from the National Key Subject of Drug Innovation (No.2019ZX09201005-007), Tianjin Outstanding Youth Science Foundation (No.17JCJQJC46200), the National Natural Science Foundation of China (No.81774050), the Natural Science Foundation of Tianjin (17JCYBJC29000).


## Author Contributions

Guanwei Fan, Xiumei Gao, Jingyuan Mao and Jingyu Ni designed experiments; Jingyu Ni, Zhihao Liu, Jie Deng and Xiaodan Wang carried out experiments; Miaomiao Jiang, Lan Li and Yan Zhu analyzed experimental results. Jingyu Ni wrote the manuscript. All authors reviewed and edited this manuscript.


## Acknowledgements

Not applicable.


## Reference


1. Katz AM, Rolett EL. Heart failure: when form fails to follow function. Eur Heart J. 2016;37:449-454.

2. Papadimitriou L, Hamo CE, Butler J. Heart failure guidelines: What's new?. Trends Cardiovasc Med. 2017;27:316-323.

3. van Bilsen M, Smeets PJ, Gilde AJ, van der Vusse GJ. Metabolic remodelling of

679 the failing heart: the cardiac burn-out syndrome?. Cardiovasc Res. 2004;61:218-226.
680 4. Ritchie RH, Delbridge LM. Cardiac hypertrophy, substrate utilization and
681 metabolic remodelling: cause or effect?. Clin Exp Pharmacol Physiol.
682 2006;33:159-166.
683 5. Doenst T, Nguyen TD, Abel ED. Cardiac metabolism in heart failure: implications
684 beyond ATP production. Circ Res. 2013;113:709-724.
685 6. Doehner W, Frenneaux M, Anker SD. Metabolic impairment in heart failure: the
686 myocardial and systemic perspective. J Am Coll Cardiol. 2014;64:1388-1400.
687 7. Lopaschuk GD, Ussher JR. Evolving Concepts of Myocardial Energy Metabolism:
688 More Than Just Fats and Carbohydrates. Circ Res. 2016;119:1173-1176.
689 8. Guo CA, Guo S. Insulin receptor substrate signaling controls cardiac energy
690 metabolism and heart failure. J Endocrinol. 2017;233:R131-R143.
691 9. Lopaschuk GD. Fatty Acid Oxidation and Its Relation with Insulin Resistance and
692 Associated Disorders. Ann Nutr Metab. 2016;68:15-20.
693 10. Patel TP, Rawal K, Bagchi AK, Akolkar G, Bernardes N, Dias DDS, Gupta S,
694 Singal PK. Insulin resistance: an additional risk factor in the pathogenesis of
695 cardiovascular disease in type 2 diabetes. Heart Fail Rev. 2016;21:11-23.
696 11. Ingelsson E, Sundström J, Arnlöv J, Zethelius B, Lind L. Insulin resistance and
697 risk of congestive heart failure. JAMA. 2005;294:334-341.
698 12. ardeny O, Gupta DK, Claggett B, Burke S, Shah A, Loehr L, Rasmussen-Torvik L,
699 Selvin E, Chang PP, Aguilar D, Solomon SD. Insulin resistance and incident heart
700 failure the ARIC study (Atherosclerosis Risk in Communities). JACC Heart Fail.

2013;1:531-6.

13. Greene SJ, Fonarow GC. Insulin resistance in heart failure: widening the divide between reduced and preserved ejection fraction?. Eur J Heart Fail. 2015;17:991-993.

14. Rask-Madsen C, Kahn CR. Tissue-specific insulin signaling, metabolic syndrome, and cardiovascular disease. Arterioscler Thromb Vasc Biol. 2012;32:2052-2059.

15. Heck PM, Dutka DP. Insulin resistance and heart failure. Curr Heart Fail Rep. 2009;6:89-94.

16. Fu F, Zhao K, Li J, Xu J, Zhang Y, Liu C, Yang W, Gao C, Li J, Zhang H, Li Y, Cui Q, Wang H, Tao L, Wang J, Quon MJ, Gao F. Direct Evidence that Myocardial Insulin Resistance following Myocardial Ischemia Contributes to Post-Ischemic Heart Failure. Sci Rep. 2015;5:17927.

17. Novo G, Manno G, Russo R, Buccheri D, Dell'Oglio S, Morreale P, Evola G, Vitale G, Novo S. Impact of insulin resistance on cardiac and vascular function. Int J Cardiol. 2016;221:1095-9.

18. Ormazabal V, Nair S, Elfeky O, Aguayo C, Salomon C, Zuñiga FA. Association between insulin resistance and the development of cardiovascular disease. Cardiovasc Diabetol. 2018;17:122.

19. Salt IP, Hardie DG. AMP-Activated Protein Kinase: An Ubiquitous Signaling Pathway With Key Roles in the Cardiovascular System. Circ Res. 2017;120:1825-1841.

20. Qi D, Young LH. AMPK: energy sensor and survival mechanism in the ischemic heart. Trends Endocrinol Metab. 2015;26:422-429.

723 21. Smith BK, Steinberg GR. AMP-activated protein kinase, fatty acid metabolism,
724 and insulin sensitivity. Curr Opin Clin Nutr Metab Care. 2017;20:248-253.
725 22. Kim J, Yang G, Kim Y, Kim J, Ha J. AMPK activators: mechanisms of action and
726 physiological activities. Exp Mol Med. 2016;48:e224.
727 23. Cheng L, Sun X, Hu C, Jin R, Sun B, Shi Y, Cui W, Zhang Y. In vivo early
728 intervention and the therapeutic effects of 20(s)-ginsenoside rg3 on hypertrophic scar
729 formation. PLoS One. 2014;9:e113640.
730 24. Cheng L , Sun X , Li B , Hu C , Yang H , Zhang Y , Cui W . Electrospun
731 Ginsenoside Rg3/poly(lactic-co-glycolic acid) fibers coated with hyaluronic acid for
732 repairing and inhibiting hypertrophic scars. J Mater Chem B. 2013;1:4428-4437.
733 25. Smith I, Williamson EM, Putnam S, Farrimond J, Whalley BJ. Effects and
734 mechanisms of ginseng and ginsenosides on cognition. Nutr Rev. 2014;72:319-333.
735 26.Li L, Ni J, Li M, Chen J, Han L, Zhu Y, Kong D, Mao J, Wang Y, Zhang B, Zhu M,
736 Gao X, Fan G. Ginsenoside Rg3 micelles mitigate doxorubicin-induced cardiotoxicity
737 and enhance its anticancer efficacy. Drug Deliv. 2017;24:1617-1630.
738 27. Li L, Wang Y, Guo R, Li S, Ni J, Gao S, Gao X, Mao J, Zhu Y, Wu P, Wang H,
739 Kong D, Zhang H, Zhu M, Fan G. Ginsenoside Rg3-loaded, reactive oxygen
740 species-responsive polymeric nanoparticles for alleviating myocardial
741 ischemia-reperfusion injury. J Control Release. 2020;317:259-272.
742 28. Tavakoli R, Nemska S, Jamshidi P, Gassmann M, Frossard N. Technique of
743 Minimally Invasive Transverse Aortic Constriction in Mice for Induction of Left
744 Ventricular Hypertrophy. J Vis Exp. 2017;127:56231.

745 29. deAlmeida AC, van Oort RJ, Wehrens XH. Transverse aortic constriction in mice.
746 J Vis Exp. 2010;38:1729.
747 30. Kirshenbaum LA, Singal PK. Antioxidant changes in heart hypertrophy:
748 significance during hypoxia-reoxygenation injury. Can J Physiol Pharmacol.
749 1992;70:1330-1335.
750 31. Chen JR, Wei J, Wang LY, Zhu Y, Li L, Olunga MA, Gao XM, Fan GW.
751 Cardioprotection against ischemia/reperfusion injury by QiShenYiQi Pill® via
752 ameliorate of multiple mitochondrial dysfunctions. Drug Des Devel Ther.
753 2015;9:3051-66.
754 32. Boutagy NE, Rogers GW, Pyne ES, Ali MM, Hulver MW, Frisard MI. Using
755 Isolated Mitochondria from Minimal Quantities of Mouse Skeletal Muscle for High
756 throughput Microplate Respiratory Measurements. J Vis Exp. 2015;105:e53216.
757 33. Dong Z, Zhao P, Xu M, Zhang C, Guo W, Chen H, Tian J, Wei H, Lu R, Cao T.
758 Astragaloside IV alleviates heart failure via activating PPARα to switch glycolysis to
759 fatty acid β-oxidation. Sci Rep. 2017;7:2691.
760 34. Bertero E, Maack C. Metabolic remodelling in heart failure. Nat Rev Cardiol.
761 2018;15:457-470.
762 35. Nakamura M, Sadoshima J. Mechanisms of physiological and pathological
763 cardiac hypertrophy. Nat Rev Cardiol. 2018;15:387-407.
764 36. Fillmore N, Levasseur JL, Fukushima A, Wagg CS, Wang W, Dyck JRB,
765 Lopaschuk GD. Uncoupling of glycolysis from glucose oxidation accompanies the
766 development of heart failure with preserved ejection fraction. Mol Med. 2018;24:3.

767 37. Gibb AA, Hill BG. Metabolic Coordination of Physiological and Pathological
768 Cardiac Remodeling. Circ Res. 2018;123:107-128.
769 38. Shao D, Tian R. Glucose Transporters in Cardiac Metabolism and Hypertrophy.
770 Compr Physiol. 2015;6:331-351.
771 39. Laakso M. Is Insulin Resistance a Feature of or a Primary Risk Factor for
772 Cardiovascular Disease?. Curr Diab Rep. 2015;15:105.
773 40. Cubbon RM, Kearney MT, Wheatcroft SB. Endothelial IGF-1 Receptor Signalling
774 in Diabetes and Insulin Resistance. Trends Endocrinol Metab. 2016;27:96-104.
775 41.Qi Y, Zhu Q, Zhang K, Thomas C, Wu Y, Kumar R, Baker KM, Xu Z, Chen S,
776 Guo S. Activation of Foxo1 by insulin resistance promotes cardiac dysfunction and
777 β-myosin heavy chain gene expression. Circ Heart Fail. 2015;8:198-208.

## Figures

**Fig. 1 Ginsenoside Rg3 reduced myocardial hypertrophy and delayed ventricular remodeling. (a)** Representative images showing gross cardiac morphology of mice in each group (n = 5). HE staining of longitudinal heart (n = 4). **(b)** Heart weights of C57BL/6 mice(n = 15-16 each group). **(c)** Left ventricular mass of C57BL/6 mice(n = 14-16 each group). **(d-e)** Systolic left ventricular volume(n = 12-15 each group) (d), Diastolic left ventricular volume(n = 13-16 each group) (e). **(f-i)** Gene expression of the ANP(n = 6-9 each group) (f), BNP(n = 7 each group) (g), β-MHC(n = 6 each group) (h) and α-SKA(n = 9-12 each group) (i). **(j-k)** WGA staining(n = 3 each group) (j), WGA staining quantification chart (n = 4 each group)(k). **(l-m)** For immunofluorescence analysis, sections were incubated with a mixture of mouse anti-goat COLIα2(n = 6 each group) (l) or COLIIIα1(n = 6 each group)(m) polyclonal antibody and rabbit anti-goat α-Skactin polyclonal antibody. $^{\#}P < 0.05$ vs sham, $^{\#\#}P < 0.01$ vs sham; $^{*}P < 0.05$ vs model, $^{**}P < 0.01$ vs model.

**Fig. 2 Ginsenoside Rg3 improved cardiac function in mice with chronic heart failure induced by TAC. (a)** Representative M-mode echocardiograms of mice in each group (n = 5-8 each group). **(b-c)** Left ventricular ejection fraction(EF%, n = 12-15 each group) and fractional shortening(FS%, n = 13-16 each group) were assessed by serial echocardiography in mice in each group; data are expressed as mean±SD. **(d)** H&E staining of transverse sections(n = 3 each group). Scale bars, 50 μm. **(e)** Left ventricular pressure-volume loops(n = 3 each group). **(f-g)** Effect on the maximum rate of left ventricle rise(n = 3-4 each group) and the maximum rate of left

ventricle fall(n = 3-4 each group). $^{\#}P < 0.05$ vs sham, $^{\#\#}P < 0.01$ vs sham; $^{*}P < 0.05$ vs model, $^{**}P < 0.01$ vs model.

**Fig. 3 Ginsenoside Rg3 improved mitochondrial ultrastructure and function in mice with chronic heart failure induced by TAC. (a)** Ultrastructural analysis of mitochondrial integrity by transmission electron microscopy(n = 3 each group). **(b)** Tetramethylrhodamine ethyl ester (TMRE) and Mitotracker double staining were performed to detect mitochondrial inner membrane permeability in isolated myocardial cells(n = 3-4 each group). **(c-f)** Oxygen consumption rate (OCR) in mitochondria isolated from the hearts of various groups was measured with a Seahorse metabolic analyzer, ATP production, spare respiratory capacity and maximal mitochondrial respiration rates were then quantified. **(g)** Representative Western immunoblots for oxidative phosphorylation (OXPHOS) complexes(n = 3 each group). **(h-l)** Bar graph showing corresponding quantitative data for Western blotting(n = 3 each group). $^{\#}P < 0.05$ vs sham, $^{\#\#}P < 0.01$ vs sham; $^{*}P < 0.05$ vs model, $^{**}P < 0.01$ vs model.

**Fig. 4 Proteomics and metabolomics results. (a-b)** Proteomics results of mice heart tissue in each group(n = 3 each group). **(c)** Metabolomics results of plasma in each group(n = 6-8 each group).

**Fig. 5 Fusion of proteomics and metabolomics data showed that ginsenoside Rg3 had a moderating effect on glycolysis/gluconeogenesis. (a)** Glycolysis/gluconeogenesis. **(b)** Glycerophospholipid metabolism. **(c)** Alanine, aspartate and glutamate metabolism.

**Fig. 6 Ginsenoside Rg3 regulated glucose uptake and myocardial insulin sensitivity in mice with heart failure. (a-b)** Quantitative analysis of energy metabolites in mouse heart tissue by LC-MS/MS. The results were quantified separately according to different metabolic pathways(n = 4 each group). **(c)** Representative Western immunoblots for GLUT4 and GLUT1(n = 3 each group). **(d-e)** Bar graph showing corresponding quantitative data for Western blotting(n = 3 each group). **(f-g)** Glucose uptake in mice were observed using 18-fluorodeoxyglucose (18-FDG) positron emission tomography (micro PET). The myocardial glucose standard uptake value (SUV) was calculated(n = 3 each group). **(h)** Representative Western immunoblots for IRS-1, Akt-1, AS160, PDK4, AMPK and GAPDH(n = 3 each group). **(i-l)** Bar graph showing corresponding quantitative data for Western blotting(n = 3 each group). $^{\#}P < 0.05$ vs sham, $^{\#\#}P < 0.01$ vs sham; $^{*}P < 0.05$ vs model, $^{**}P < 0.01$ vs model.

**Fig. 7 The effect of ginsenoside Rg3 on the promotion of glucose uptake in IR-H9c2 cells by AMPK activation was dependent on the insulin signaling pathway. (a)** The cell viability was detected by MTT assay(n = 10-12 each group). **(b)** Representative Western immunoblots for p-AMPK and t-AMPK in normal H9c2 cells(n = 3 each group). **(c)** Bar graph showing corresponding quantitative data for Western blotting(n = 3 each group). **(d)** Representative Western immunoblots for p-AMPK and t-AMPK in IR-H9c2 cardiomyocytes(n = 3 each group). **(e)** Bar graph showing corresponding quantitative data for Western blotting(n = 3 each group). **(f-g)** Glucose uptake in IR-H9c2 cardiomyocytes was evaluated using 2-NBDG fluorescent

probes(n = 3 each group).

**Fig. 1**

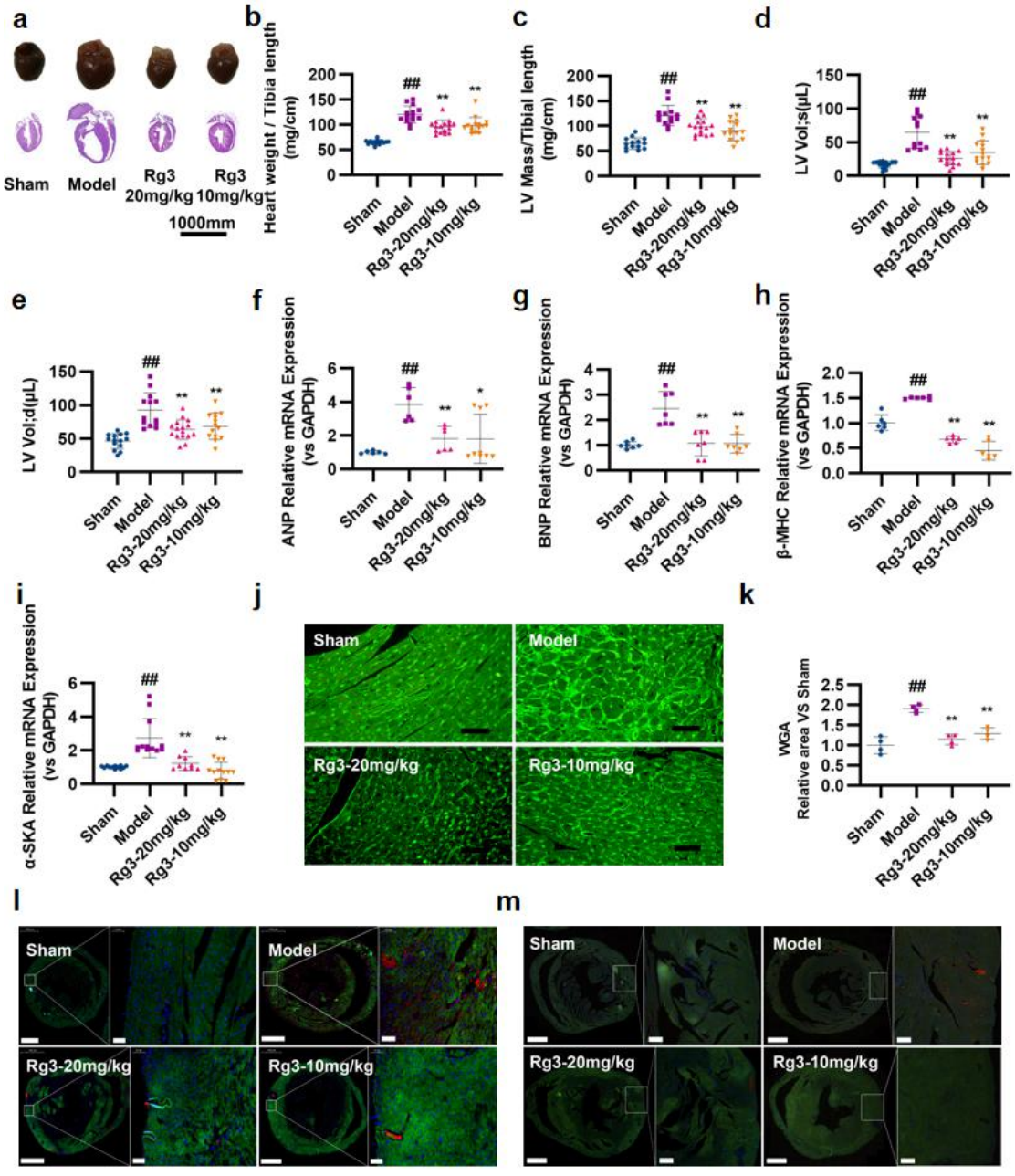
a
Sham
Model
Rg3 20mg/kg
Rg3 10mg/kg
1000mm
b
Heart weight / Tibia length (mg/cm)
c
LV Mass/Tibial length (mg/cm)
d
LV Vol;s(μL)
e
LV Vol;d(μL)
f
ANP Relative mRNA Expression (vs GAPDH)
g
BNP Relative mRNA Expression (vs GAPDH)
h
β-MHC Relative mRNA Expression (vs GAPDH)
i
α-SKA Relative mRNA Expression (vs GAPDH)
j
Sham
Model
Rg3-20mg/kg
Rg3-10mg/kg
k
WGA
Relative area VS Sham
l
m
Sham
Model
Rg3-20mg/kg
Rg3-10mg/kg

873 **Fig. 2**

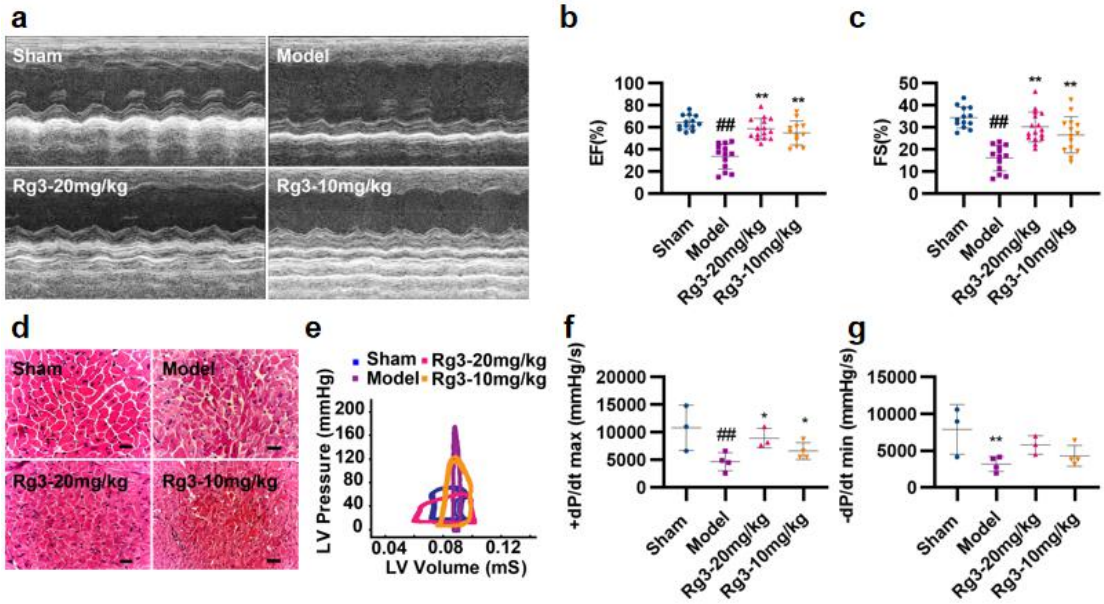


874

875

876

877

878 **Fig. 3**

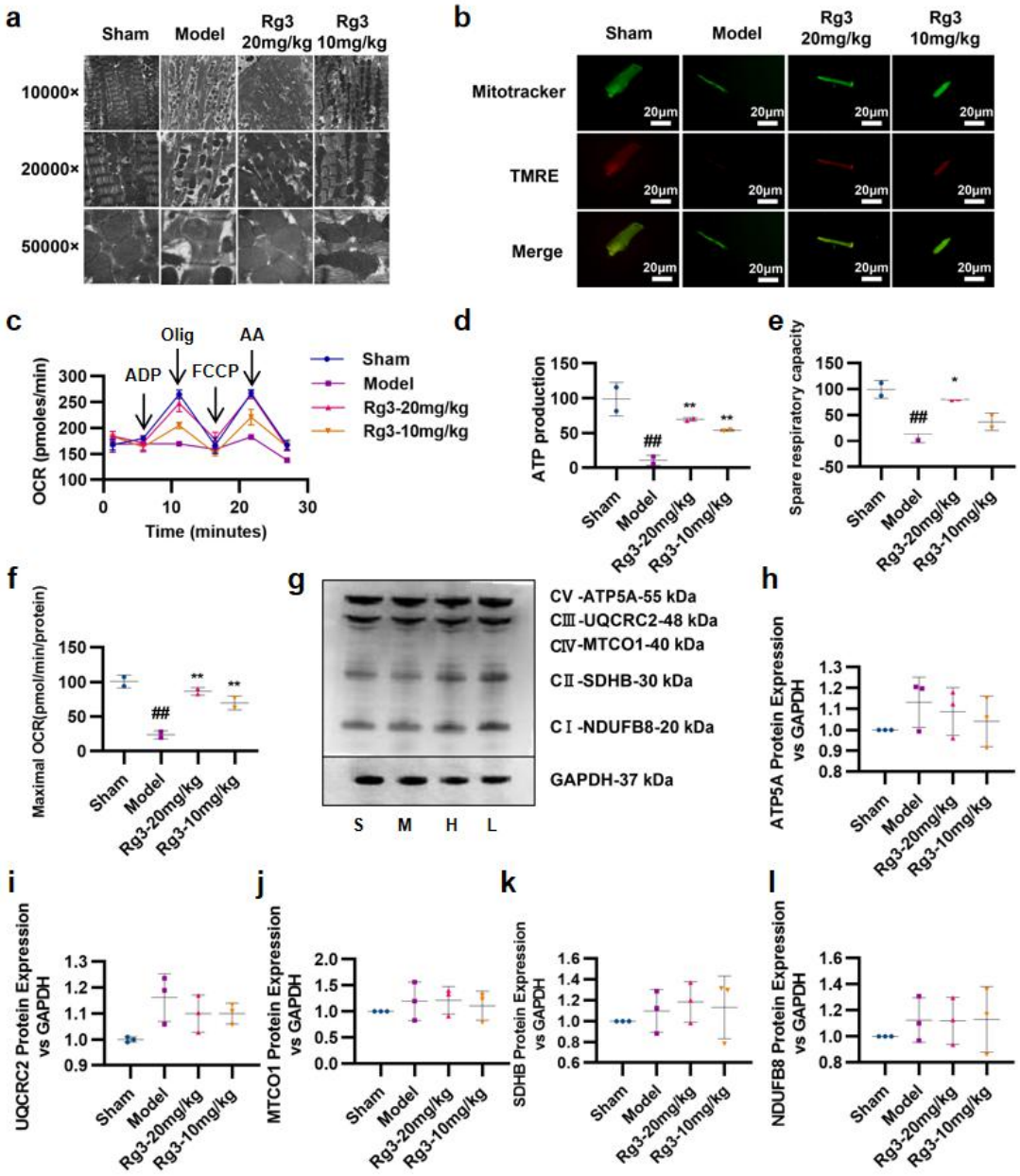


879

880

881 **Fig. 4**

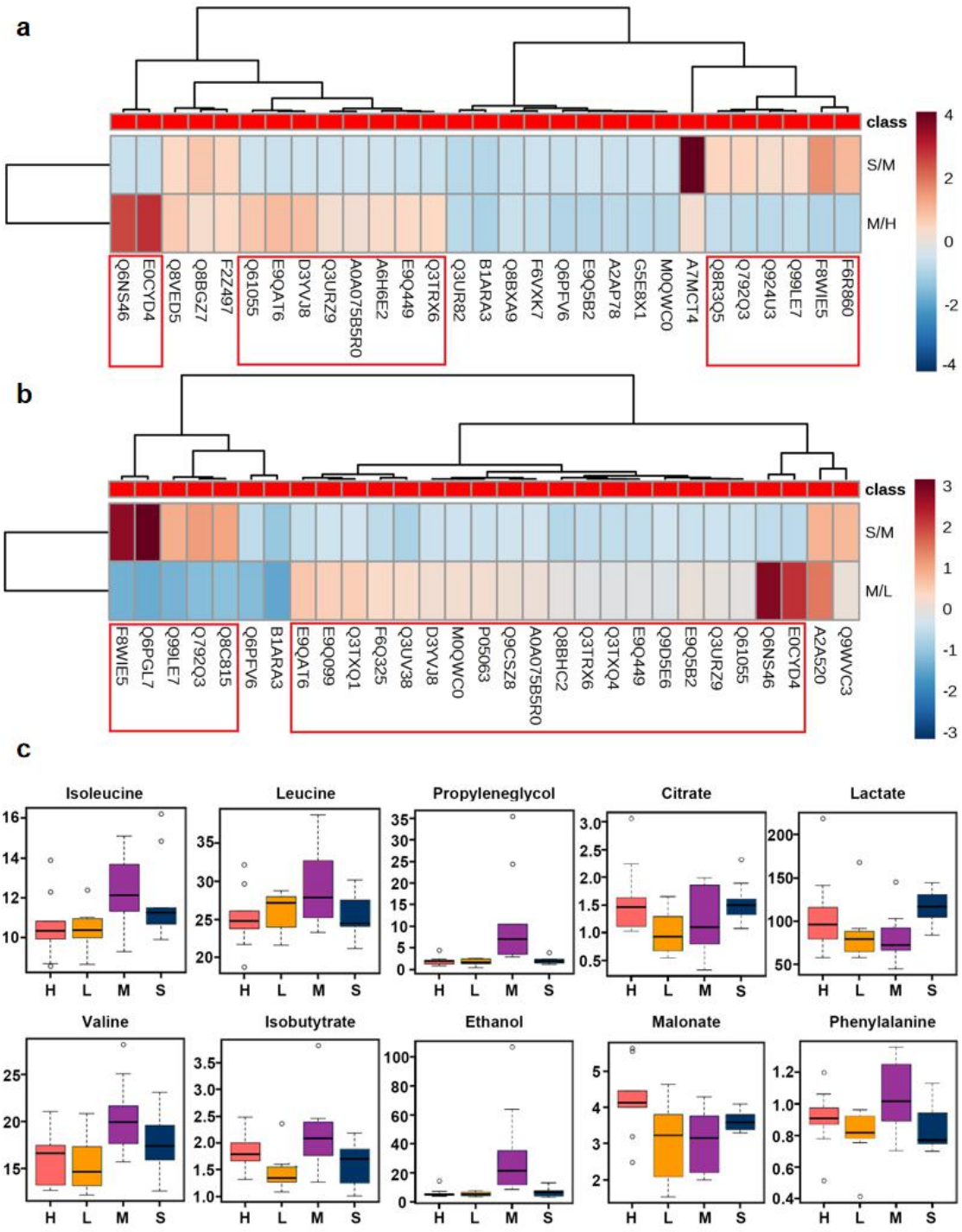


882

883

884

**Fig. 5**

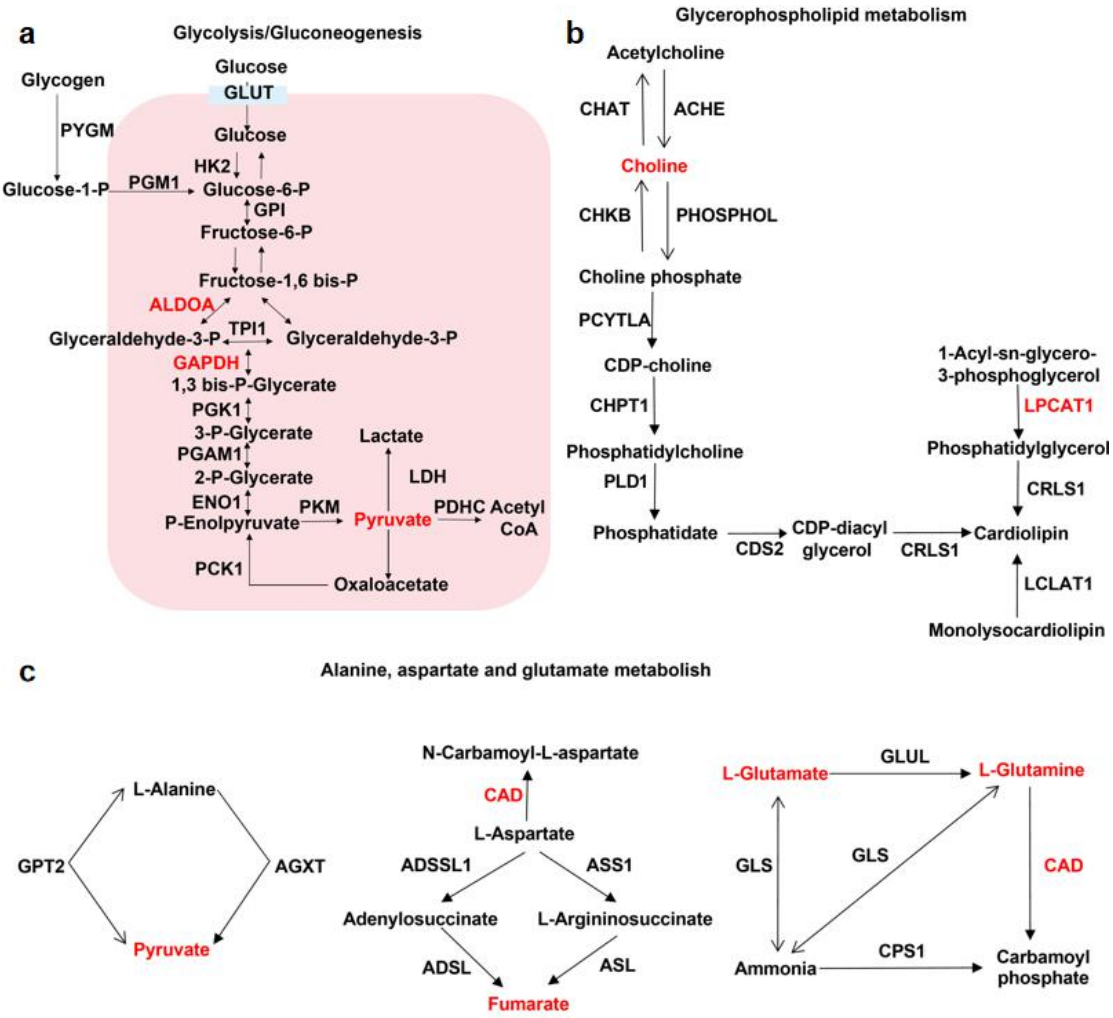
a
Glycolysis/Gluconeogenesis
Glycogen
PYGM
Glucose
GLUT
Glucose
HK2
Glucose-1-P
PGM1
Glucose-6-P
GPI
Fructose-6-P
Fructose-1,6 bis-P
ALDOA
TPI1
Glyceraldehyde-3-P
Glyceraldehyde-3-P
GAPDH
1,3 bis-P-Glycerate
PGK1
3-P-Glycerate
PGAM1
2-P-Glycerate
ENO1
P-Enolpyruvate
PKM
Pyruvate
Lactate
LDH
PDHC
Acetyl CoA
PCK1
Oxaloacetate
b
Glycerophospholipid metabolism
Acetylcholine
CHAT
ACHE
Choline
CHKB
PHOSPHOL
Choline phosphate
PCYTLA
CDP-choline
CHPT1
Phosphatidylcholine
PLD1
Phosphatidate
CDS2
CDP-diacyl glycerol
CRLS1
Cardiolipin
1-Acyl-sn-glycero-3-phosphoglycerol
LPCAT1
Phosphatidylglycerol
CRLS1
LCLAT1
Monolysocardiolipin
c
Alanine, aspartate and glutamate metabolish
L-Alanine
GPT2
AGXT
Pyruvate
N-Carbamoyl-L-aspartate
CAD
L-Aspartate
ADSSL1
ASS1
Adenylosuccinate
L-Argininosuccinate
ADSL
ASL
Fumarate
L-Glutamate
GLUL
L-Glutamine
GLS
GLS
CAD
Ammonia
CPS1
Carbamoyl phosphate

**Fig. 6**

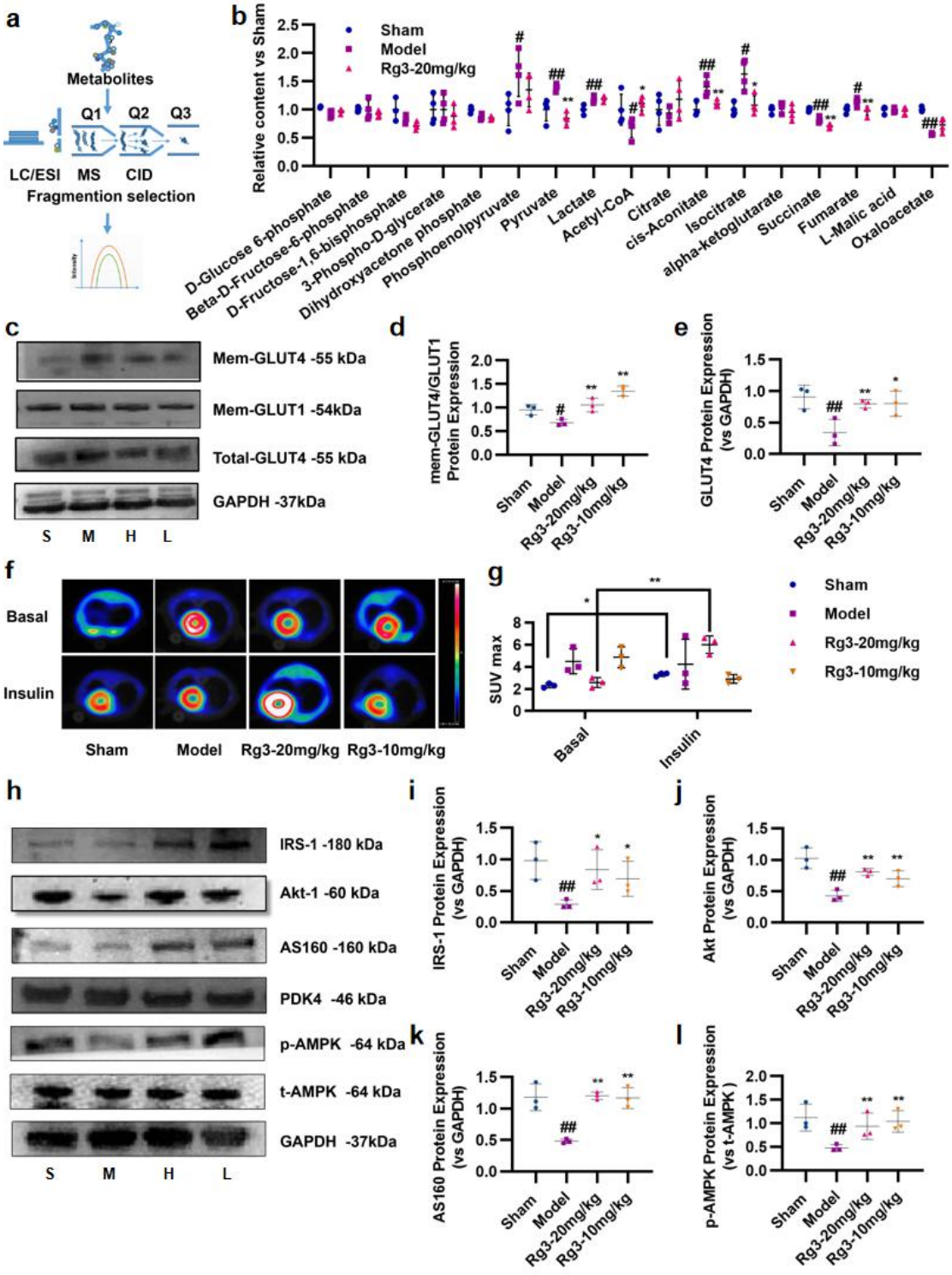
a
Metabolites
Q1
Q2
Q3
LC/ESI
MS
CID
Fragmention selection
b
Relative content vs Sham
Sham
Model
Rg3-20mg/kg
D-Glucose 6-phosphate
Beta-D-Fructose-6-phosphate
D-Fructose-1,6-bisphosphate
3-Phospho-D-glycerate
Dihydroxyacetone phosphate
Phosphoenolpyruvate
Pyruvate
Lactate
Acetyl-CoA
Citrate
cis-Aconitate
Isocitrate
alpha-ketoglutarate
Succinate
Fumarate
L-Malic acid
Oxaloacetate
c
Mem-GLUT4 -55 kDa
Mem-GLUT1 -54kDa
Total-GLUT4 -55 kDa
GAPDH -37kDa
S
M
H
L
d
mem-GLUT4/GLUT1 Protein Expression
e
GLUT4 Protein Expression (vs GAPDH)
f
Basal
Insulin
Sham
Model
Rg3-20mg/kg
Rg3-10mg/kg
g
SUV max
Basal
Insulin
h
IRS-1 -180 kDa
Akt-1 -60 kDa
AS160 -160 kDa
PDK4 -46 kDa
p-AMPK -64 kDa
t-AMPK -64 kDa
GAPDH -37kDa
i
IRS-1 Protein Expression (vs GAPDH)
j
Akt Protein Expression (vs GAPDH)
k
AS160 Protein Expression (vs GAPDH)
l
p-AMPK Protein Expression (vs t-AMPK)

**Fig. 7**

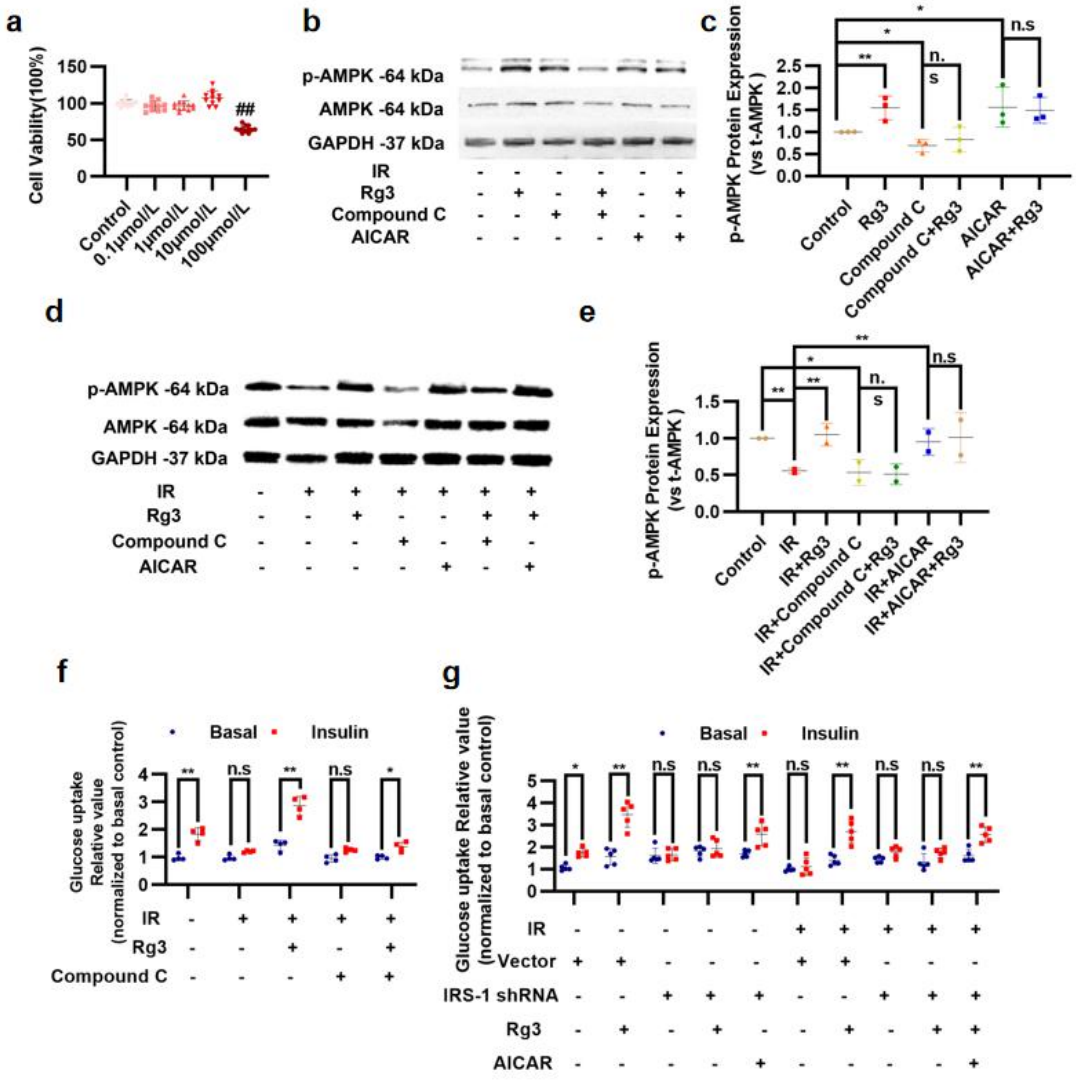
a
Cell Vability(100%)
150
100
50
0
##
Control
0.1μmol/L
1μmol/L
10μmol/L
100μmol/L
b
p-AMPK -64 kDa
AMPK -64 kDa
GAPDH -37 kDa
IR
Rg3
Compound C
AICAR
c
p-AMPK Protein Expression (vs t-AMPK)
n.s
Control
Rg3
Compound C
Compound C+Rg3
AICAR
AICAR+Rg3
d
p-AMPK -64 kDa
AMPK -64 kDa
GAPDH -37 kDa
IR
Rg3
Compound C
AICAR
e
p-AMPK Protein Expression (vs t-AMPK)
n.s
Control
IR
IR+Rg3
IR+Compound C
IR+Compound C+Rg3
IR+AICAR
IR+AICAR+Rg3
f
Basal
Insulin
Glucose uptake Relative value (normalized to basal control)
n.s
IR
Rg3
Compound C
g
Basal
Insulin
Glucose uptake Relative value (normalized to basal control)
n.s
IR
Vector
IRS-1 shRNA
Rg3
AICAR

**Fig. 8**

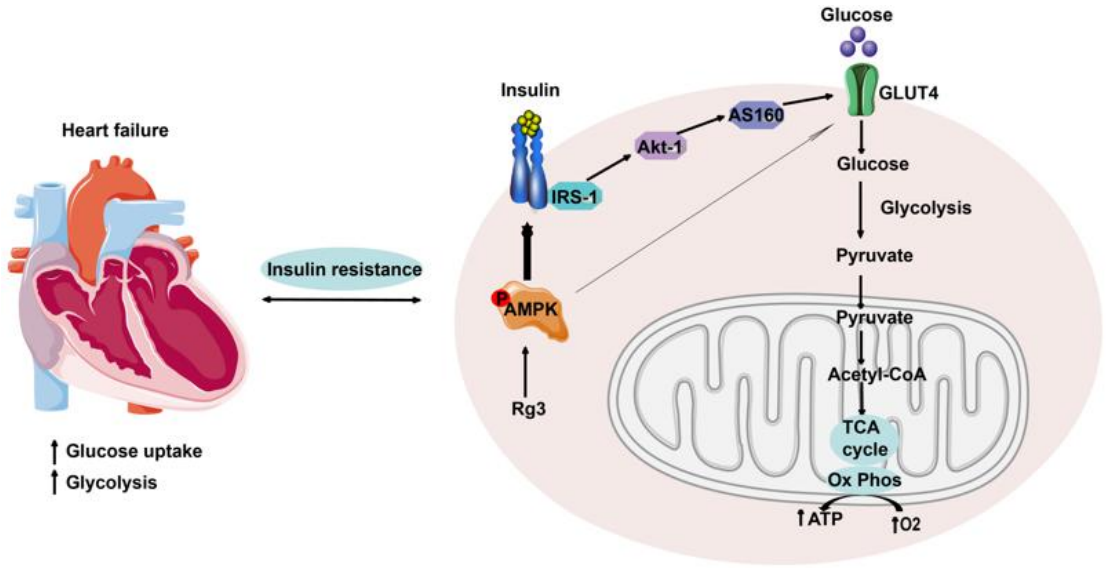
Heart failure
Glucose uptake
Glycolysis
Insulin resistance
Insulin
IRS-1
Akt-1
AS160
GLUT4
Glucose
Glycolysis
Pyruvate
Pyruvate
Acetyl-CoA
TCA cycle
Ox Phos
ATP
O2
AMPK
Rg3

**Table 1 RT-PCR primers**

| Primers | Sequence of the primers |
|---|---|
| ANP | 5'-TGG GAC CCC TCC GAT AGA TC-3' |
| | 5'-TCG TGA TAG ATG AAG GCA GGA A-3' |
| BNP | 5'-GGAAGTCAACGGGAAGAAGTTCACTG-3' |
| | 5'-CAATGTAACCGGCACCCACAATAAC-3' |
| β-MHC | 5'-TTG AGA ATC CAA GGC TCA GC-3' |
| | 5'-CTT CTC AGA CTT CCG CAG GA-3' |
| α-SKA | 5'-CAG CTC TGG CTC CCA GCA CC-3' |
| | 5'-AAT GGC TGG CTT TAA TGC TTC A-3' |
| GAPDH | 5'-CGG CCG CAT CTT CTT GTG-3' |
| | 5'-CAC CGA CCT TCA CCA TTT TGT-3' |

927 **Table 2 Differential proteins regulated by ginsenoside Rg3-20mg/kg**

| Accession | GN | Description |
|---|---|---|
| Q8R3Q5 | Ppp1r37 | Lrrc68 protein OS=Mus musculus GN=Ppp1r37 PE=2 SV=1 - [Q8R3Q5_MOUSE] |
| Q792Q3 | C2 | Complement factor C2 (Fragment) OS=Mus musculus GN=C2 PE=3 SV=1 - [Q792Q3_MOUSE] |
| F8WIE5 | Hectd1 | E3 ubiquitin-protein ligase HECTD1 OS=Mus musculus GN=Hectd1 PE=1 SV=1 - [F8WIE5_MOUSE] |
| Q924U3 | Caveolin | Caveolin (Fragment) OS=Mus musculus PE=3 SV=1 - [Q924U3_MOUSE] |
| Q99LE7 | Pxn | Pxn protein (Fragment) OS=Mus musculus GN=Pxn PE=2 SV=1 - [Q99LE7_MOUSE] |
| F6R860 | Wdsub1 | WD repeat, SAM and U-box domain-containing protein 1 (Fragment) OS=Mus musculus GN=Wdsub1 PE=1 SV=1 - [F6R860_MOUSE] |
| Q6NS46 | Pdcd11 | Protein RRP5 homolog OS=Mus musculus GN=Pdcd11 PE=1 SV=2 - [RRP5_MOUSE] |
| E9Q449 | Dennd4c | DENN domain-containing protein 4C OS=Mus musculus GN=Dennd4c PE=1 SV=1 - [E9Q449_MOUSE] |
| E9QAT6 | Cad | CAD protein OS=Mus musculus GN=Cad PE=1 SV=1 - [E9QAT6_MOUSE] |
| Q3URZ9 | Cspg4 | Putative uncharacterized protein (Fragment) OS=Mus musculus GN=Cspg4 PE=2 SV=1 - [Q3URZ9_MOUSE] |
| E0CYD4 | Gtf2a1l | TFIIA-alpha and beta-like factor (Fragment) OS=Mus musculus GN=Gtf2a1l PE=1 SV=7 - [E0CYD4_MOUSE] |
| Q3TRX6 | Dnajc2 | DnaJ homolog subfamily C member 2 OS=Mus musculus GN=Dnajc2 PE=1 SV=1 - [Q3TRX6_MOUSE] |
| D3YVJ8 | Rdh13 | Retinol dehydrogenase 13 (Fragment) OS=Mus musculus GN=Rdh13 PE=1 SV=1 - [D3YVJ8_MOUSE] |
| A0A075B5R0 | Ighv5-16 | Protein Ighv5-16 OS=Mus musculus GN=Ighv5-16 PE=1 SV=1 - [A0A075B5R0_MOUSE] |
| A6H6E2 | Mmrn2 | Multimerin-2 OS=Mus musculus GN=Mmrn2 PE=1 SV=1 - [MMRN2_MOUSE] |
| Q61055 | Abl2 | Protein tyrosine kinase (Fragment) OS=Mus musculus GN=Abl2 PE=2 SV=1 - [Q61055_MOUSE] |

928

929

930

931

**Table 3 Differential proteins regulated by ginsenoside Rg3-10mg/kg**

| Accession | GN | Description |
|---|---|---|
| Q792Q3 | C2 | Complement factor C2 (Fragment) OS=Mus musculus GN=C2 PE=3 SV=1 - [Q792Q3_MOUSE] |
| F8WIE5 | Hectd1 | E3 ubiquitin-protein ligase HECTD1 OS=Mus musculus GN=Hectd1 PE=1 SV=1 - [F8WIE5_MOUSE] |
| Q99LE7 | Pxn | Pxn protein (Fragment) OS=Mus musculus GN=Pxn PE=2 SV=1 - [Q99LE7_MOUSE] |
| E9Q5B2 | 0610011F06 Rik | Protein 0610011F06Rik OS=Mus musculus GN=0610011F06Rik PE=1 SV=1 - [E9Q5B2_MOUSE] |
| M0QWC0 | Rpgrip1 | X-linked retinitis pigmentosa GTPase regulator-interacting protein 1 OS=Mus musculus GN=Rpgrip1 PE=4 SV=1 - [M0QWC0_MOUSE] |
| Q8C815 | | Putative uncharacterized protein OS=Mus musculus PE=2 SV=1 - [Q8C815_MOUSE] |
| Q6PGL7 | Fam21 | WASH complex subunit FAM21 OS=Mus musculus GN=Fam21 PE=1 SV=1 - [FAM21_MOUSE] |
| Q9D5E6 | 4930449A1 8Rik | MCG13105, isoform CRA_b OS=Mus musculus GN=4930449A18Rik PE=2 SV=1 - [Q9D5E6_MOUSE] |
| Q3TXQ4 | Npc2 | Putative uncharacterized protein OS=Mus musculus GN=Npc2 PE=2 SV=1 - [Q3TXQ4_MOUSE] |
| Q8BHC2 | Ist1 | 2400003C14Rik protein OS=Mus musculus GN=Ist1 PE=2 SV=1 - [Q8BHC2_MOUSE] |
| F6Q325 | Nde1 | Nuclear distribution protein nudE homolog 1 (Fragment) OS=Mus musculus GN=Nde1 PE=1 SV=1 - [F6Q325_MOUSE] |
| Q3UV38 | Tpcn1 | Putative uncharacterized protein (Fragment) OS=Mus musculus GN=Tpcn1 PE=2 SV=1 - [Q3UV38_MOUSE] |
| P05063 | Aldoc | Fructose-bisphosphate aldolase C OS=Mus musculus GN=Aldoc PE=1 SV=4 - [ALDOC_MOUSE] |
| E9Q099 | Ovgp1 | Oviduct-specific glycoprotein OS=Mus musculus GN=Ovgp1 PE=1 SV=1 - [E9Q099_MOUSE] |
| Q9CSZ8 | Mrpl45 | Putative uncharacterized protein (Fragment) OS=Mus musculus GN=Mrpl45 PE=2 SV=1 - [Q9CSZ8_MOUSE] |
| Q3TXQ1 | Tmpo | Putative uncharacterized protein OS=Mus musculus GN=Tmpo PE=2 SV=1 - [Q3TXQ1_MOUSE] |
| Q6NS46 | Pdcd11 | Protein RRP5 homolog OS=Mus musculus GN=Pdcd11 PE=1 SV=2 - [RRP5_MOUSE] |

| | | |
|---|---|---|
| E9Q449 | Dennd4c | DENN domain-containing protein 4C OS=Mus musculus GN=Dennd4c PE=1 SV=1 - [E9Q449_MOUSE] |
| E9QAT6 | Cad | CAD protein OS=Mus musculus GN=Cad PE=1 SV=1 - [E9QAT6_MOUSE] |
| Q3URZ9 | Cspg4 | Putative uncharacterized protein (Fragment) OS=Mus musculus GN=Cspg4 PE=2 SV=1 - [Q3URZ9_MOUSE] |
| E0CYD4 | Gtf2a1l | TFIIA-alpha and beta-like factor (Fragment) OS=Mus musculus GN=Gtf2a1l PE=1 SV=7 - [E0CYD4_MOUSE] |
| Q3TRX6 | Dnajc2 | DnaJ homolog subfamily C member 2 OS=Mus musculus GN=Dnajc2 PE=1 SV=1 - [Q3TRX6_MOUSE] |
| D3YVJ8 | Rdh13 | Retinol dehydrogenase 13 (Fragment) OS=Mus musculus GN=Rdh13 PE=1 SV=1 - [D3YVJ8_MOUSE] |
| A0A075B5R0 | Ighv5-16 | Protein Ighv5-16 OS=Mus musculus GN=Ighv5-16 PE=1 SV=1 - [A0A075B5R0_MOUSE] |
| Q61055 | Abl2 | Protein tyrosine kinase (Fragment) OS=Mus musculus GN=Abl2 PE=2 SV=1 - [Q61055_MOUSE] |

# Figures

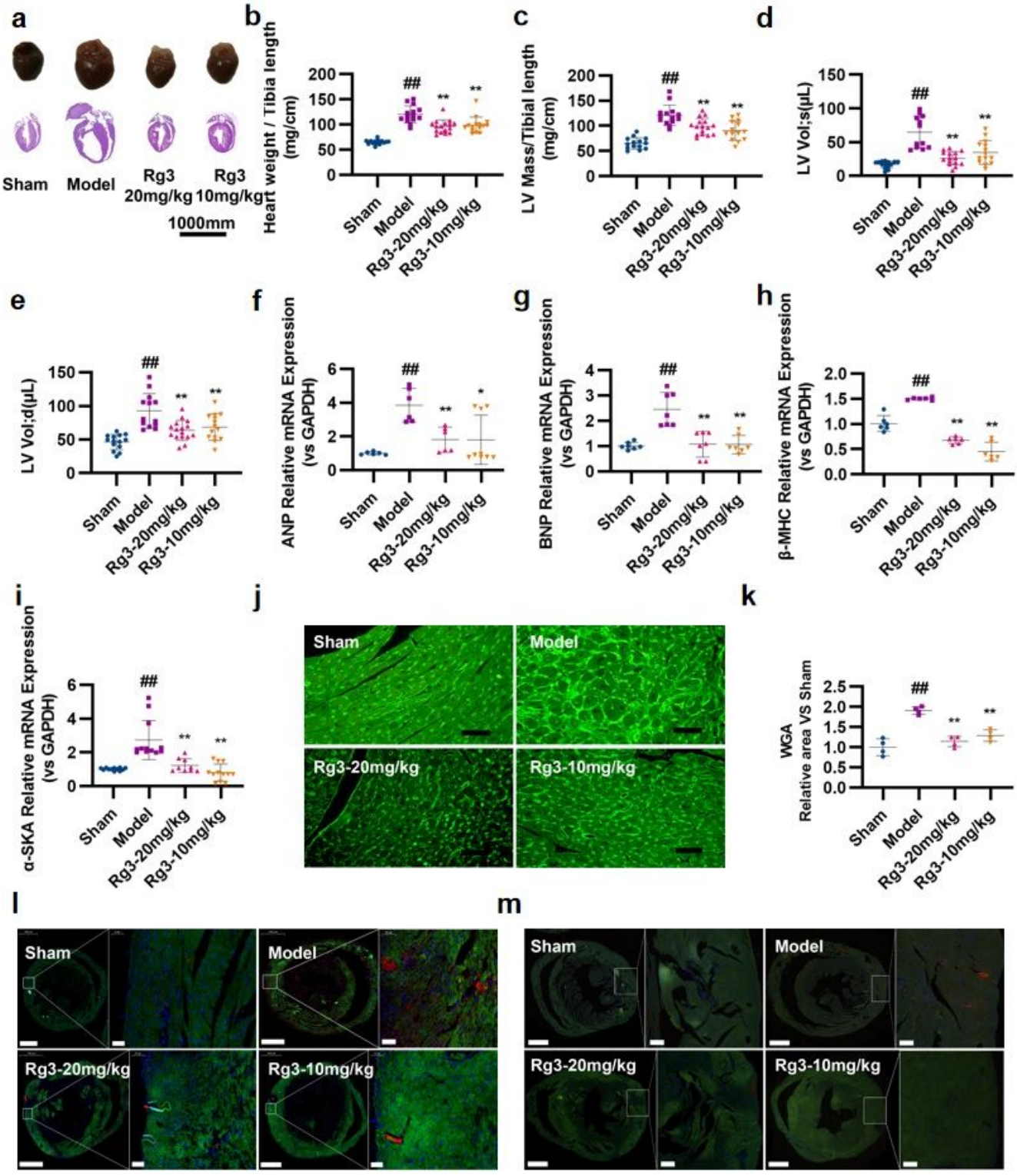


**Figure 1**

Ginsenoside Rg3 reduced myocardial hypertrophy and delayed ventricular remodeling. (a) Representative images showing gross cardiac morphology of mice in each group (n=5). HE staining of longitudinal heart (n=4). (b) Heart weights of C57BL/6 mice(n=15-16 each group). (c) Left ventricular mass of C57BL/6

mice(n 14-16 each group). (d-e) Systolic left ventricular volume(n12-15 each group) (d), Diastolic left ventricular volume(n13-16 each group) (e). (f-i) Gene expression of the ANP(n6-9 each group) (f), BNP(n7 each group) (g), β-MHC(n6 each group) (h) and α-SKA(n9-12 each group) (i). (j-k) WGA staining(n3 each group) (j), WGA staining quantification chart (n  4 each group)(k). (l-m) For immunofluorescence analysis, sections were incubated with a mixture of mouse anti-goat COLIα2(n6 each group) (l) or COLα1(n6 each group)(m) polyclonal antibody and rabbit anti-goat α-Skactin polyclonal antibody. #P0.05 vs sham, ##P 0.01 vs sham; *P0.05 vs model, **P0.01 vs model.

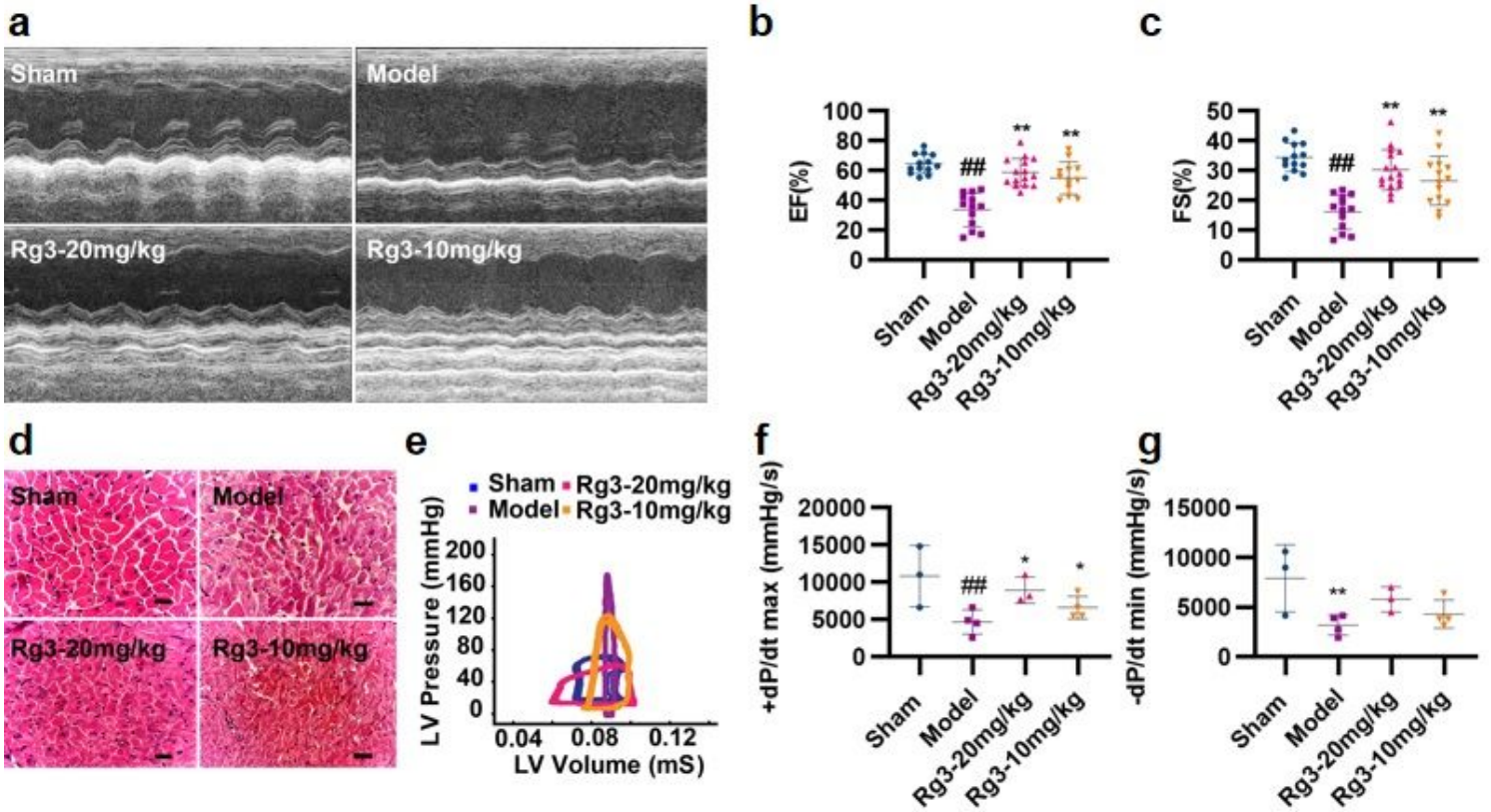


## Figure 2

Ginsenoside Rg3 improved cardiac function in mice with chronic heart failure induced by TAC. (a) Representative M-mode echocardiograms of mice in each group (n5-8 each group). (b-c) Left ventricular ejection fraction(EF%, n 12-15 each group) and fractional shortening(FS%, n  13-16 each group) were assessed by serial echocardiography in mice in each group; data are expressed as mean±SD. (d) H&E staining of transverse sections(n3 each group). Scale bars, 50 μm. (e) Left ventricular pressure-volume loops(n3 each group). (f-g) Effect on the maximum rate of left ventricle rise(n3-4 each group) and the maximum rate of left ventricle fall(n3-4 each group). #P0.05 vs sham, ##P 0.01 vs sham; *P0.05 vs model, **P0.01 vs model.

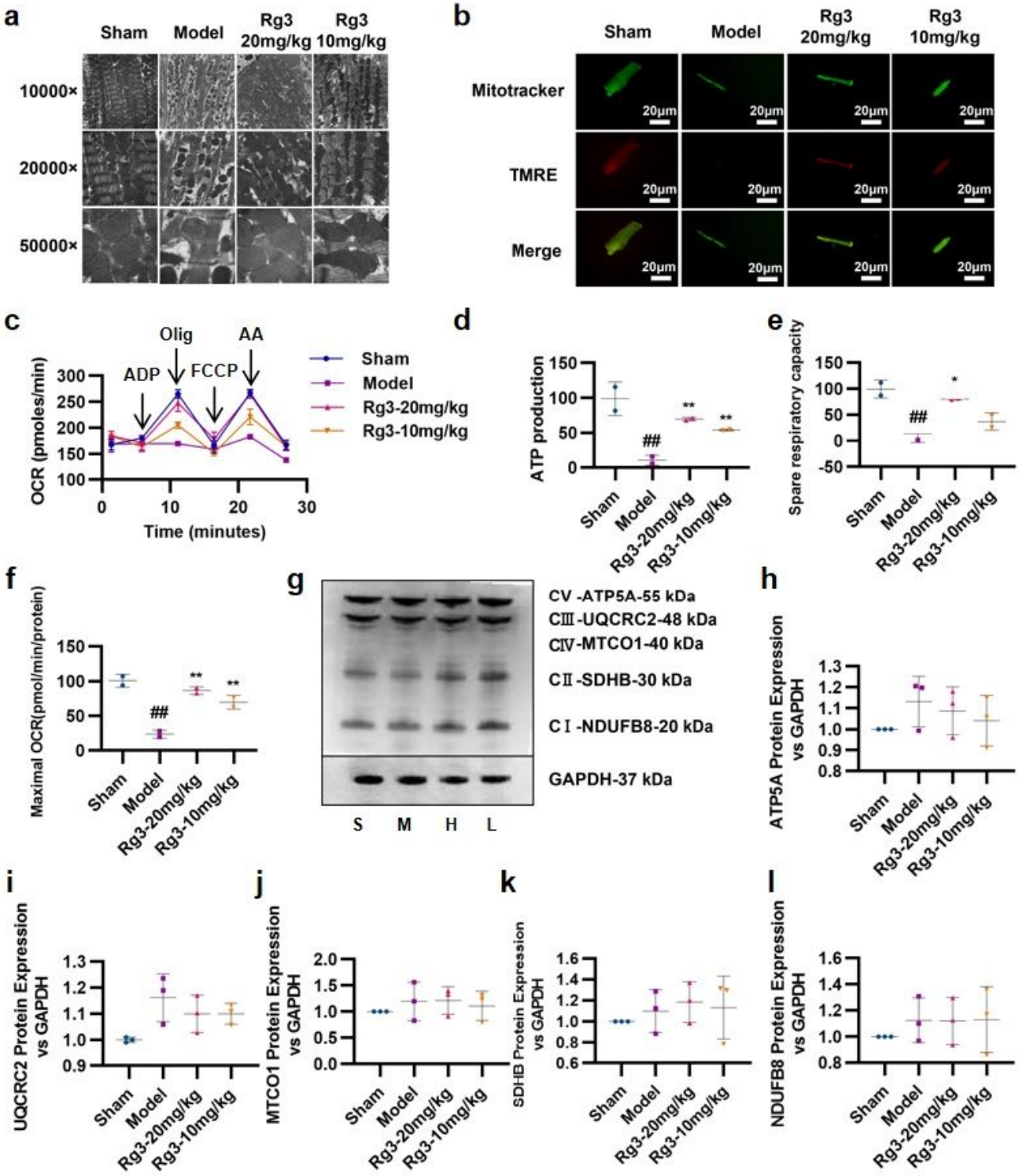


## Figure 3

Ginsenoside Rg3 improved mitochondrial ultrastructure and function in mice with chronic heart failure induced by TAC. (a) Ultrastructural analysis of mitochondrial integrity by transmission electron microscopy(n=3 each group). (b) Tetramethylrhodamine ethyl ester (TMRE) and Mitotracker double staining were performed to detect mitochondrial inner membrane permeability in isolated myocardial cells(n = 3-4 each group). (c-f) Oxygen consumption rate (OCR) in mitochondria isolated from the hearts

of various groups was measured with a Seahorse metabolic analyzer, ATP production, spare respiratory capacity and maximal mitochondrial respiration rates were then quantified. (g) Representative Western immunoblots for oxidative phosphorylation (OXPHOS) complexes(n=3 each group). (h-l) Bar graph showing corresponding quantitative data for Western blotting(n=3 each group). #P<0.05 vs sham, ##P<0.01 vs sham; *P<0.05 vs model, **P<0.01 vs model.

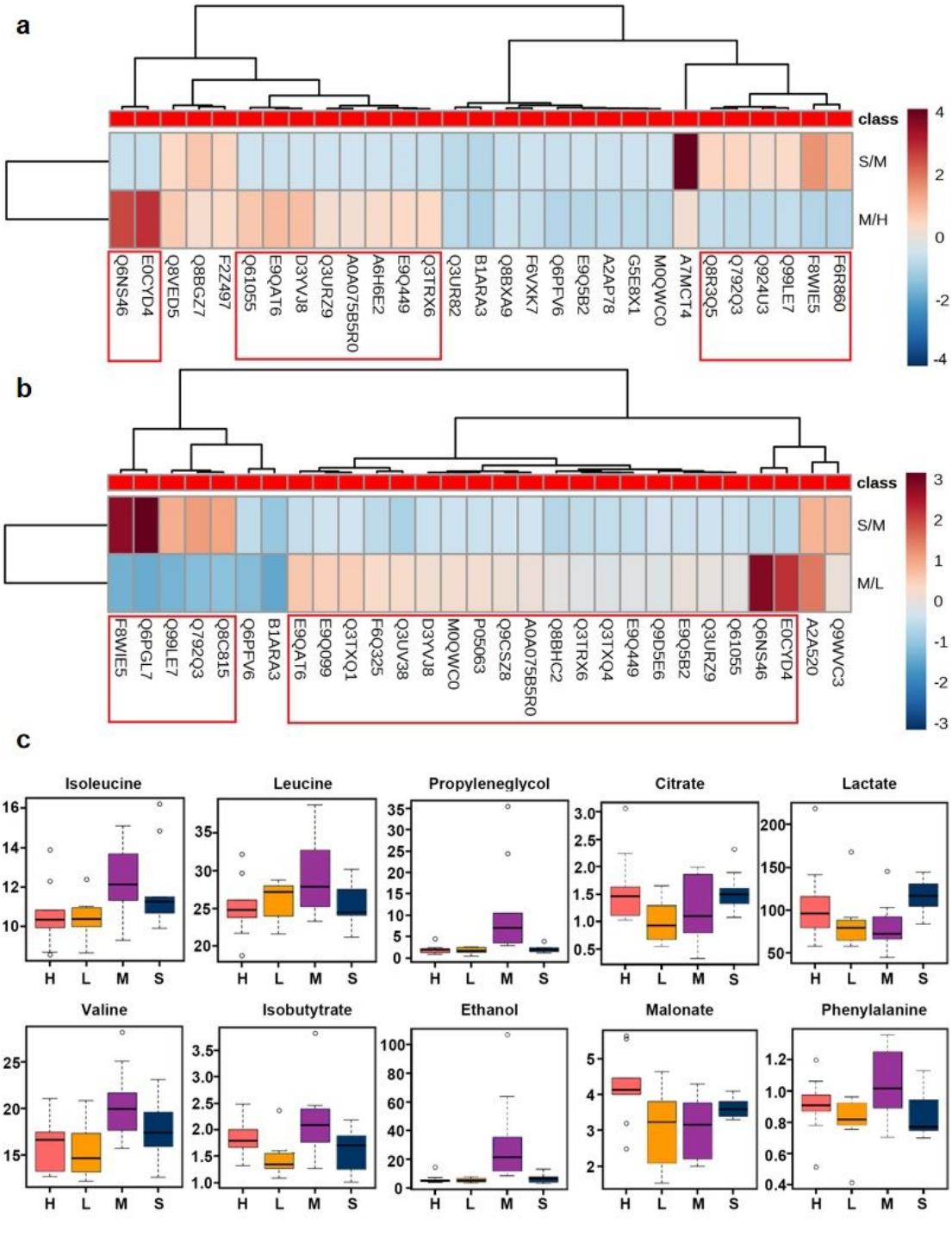


Figure 4

Proteomics and metabolomics results. (a-b) Proteomics results of mice heart tissue in each group(n=3 each group). (c) Metabolomics results of plasma in each group(n=6-8 each group).

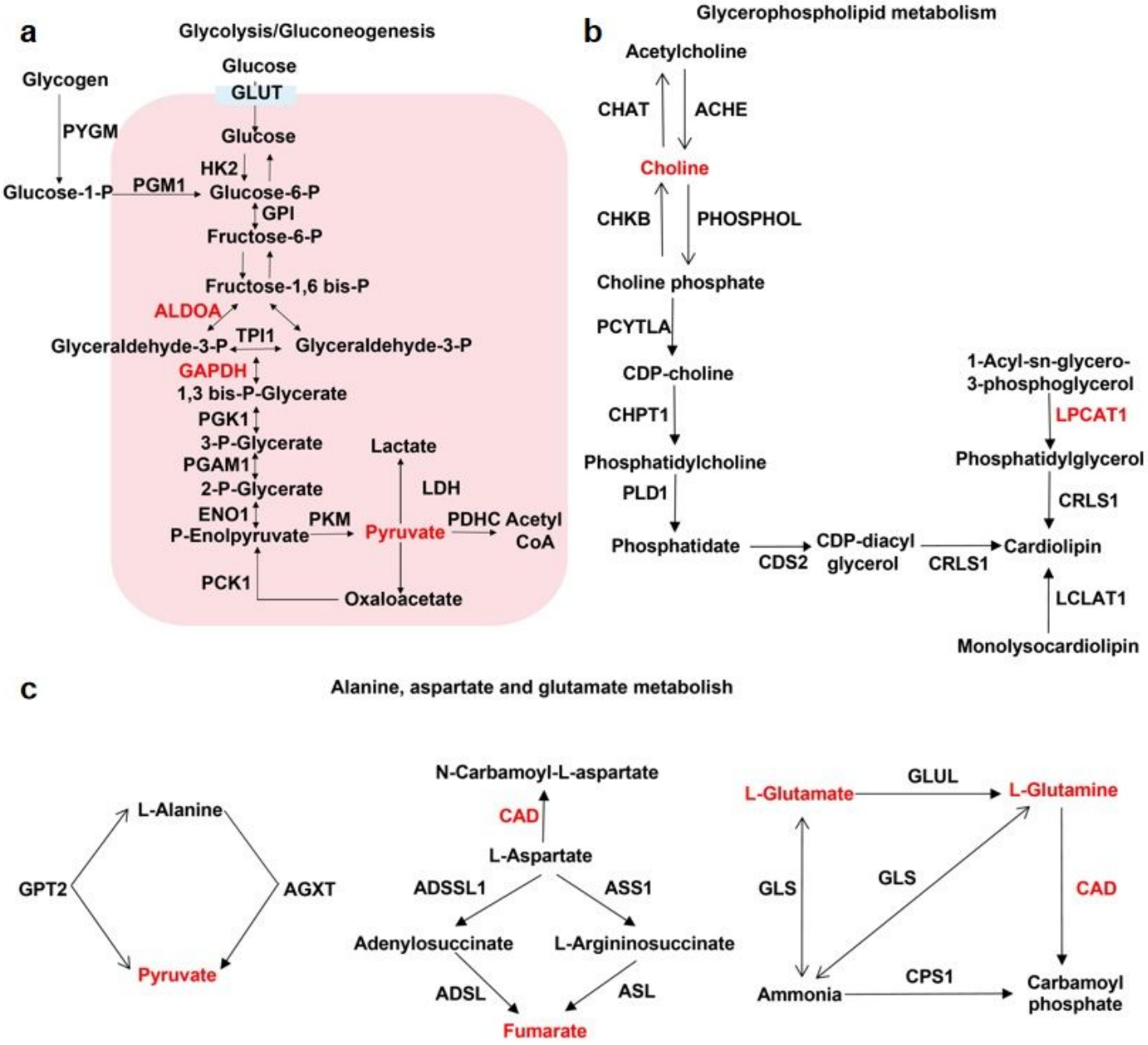


## Figure 5

Fusion of proteomics and metabolomics data showed that ginsenoside Rg3 had a moderating effect on glycolysis/gluconeogenesis. (a) Glycolysis/gluconeogenesis. (b) Glycerophospholipid metabolism. (c) Alanine, aspartate and glutamate metabolism.

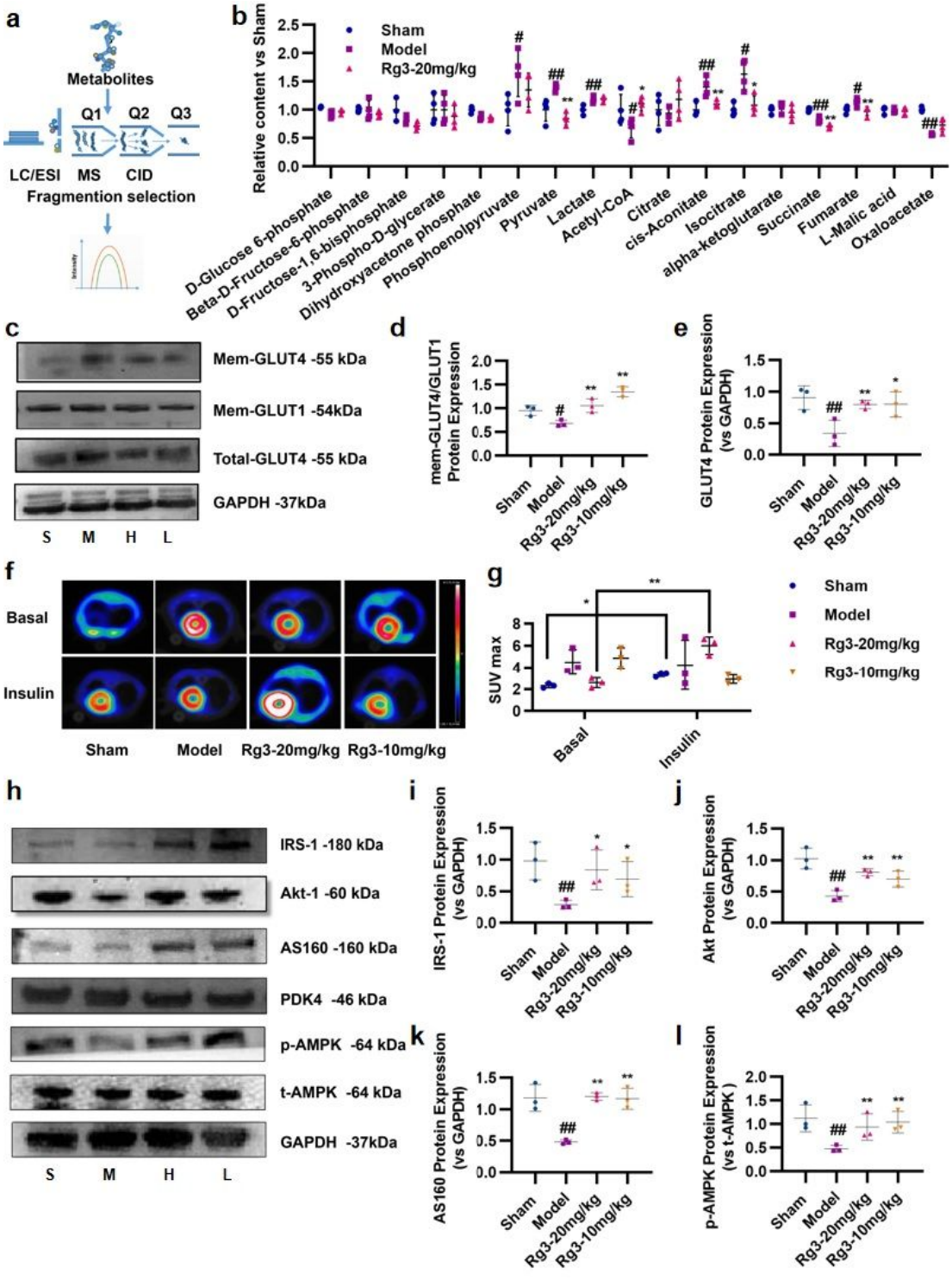


## Figure 6

Ginsenoside Rg3 regulated glucose uptake 822 and myocardial insulin sensitivity in mice with heart failure. (a-b) Quantitative analysis of energymetabolites in mouse heart tissue by LC-MS/MS. The results were quantified separately according to different metabolic pathways(n  4 each group). (c) Representative Western immunoblots for GLUT4 and GLUT1(n3 each group). (d-e) Bar graph showing corresponding quantitative data for Western blotting(n3 each group). (f-g) Glucose uptake in mice were

observed using 18-fluorodeoxyglucose (18-FDG) positron emission tomography (micro PET). The myocardial glucose standard uptake value (SUV) was calculated(n=3 each group). (h) Representative Western immunoblots for IRS-1, Akt-1, AS160, PDK4, AMPK and GAPDH(n=3 each group). (i-l) Bar graph showing corresponding quantitative data for Western blotting(n=3 each group). #P<0.05 vs sham, ##P<0.01 vs sham; *P<0.05 vs model, **P<0.01 vs model.

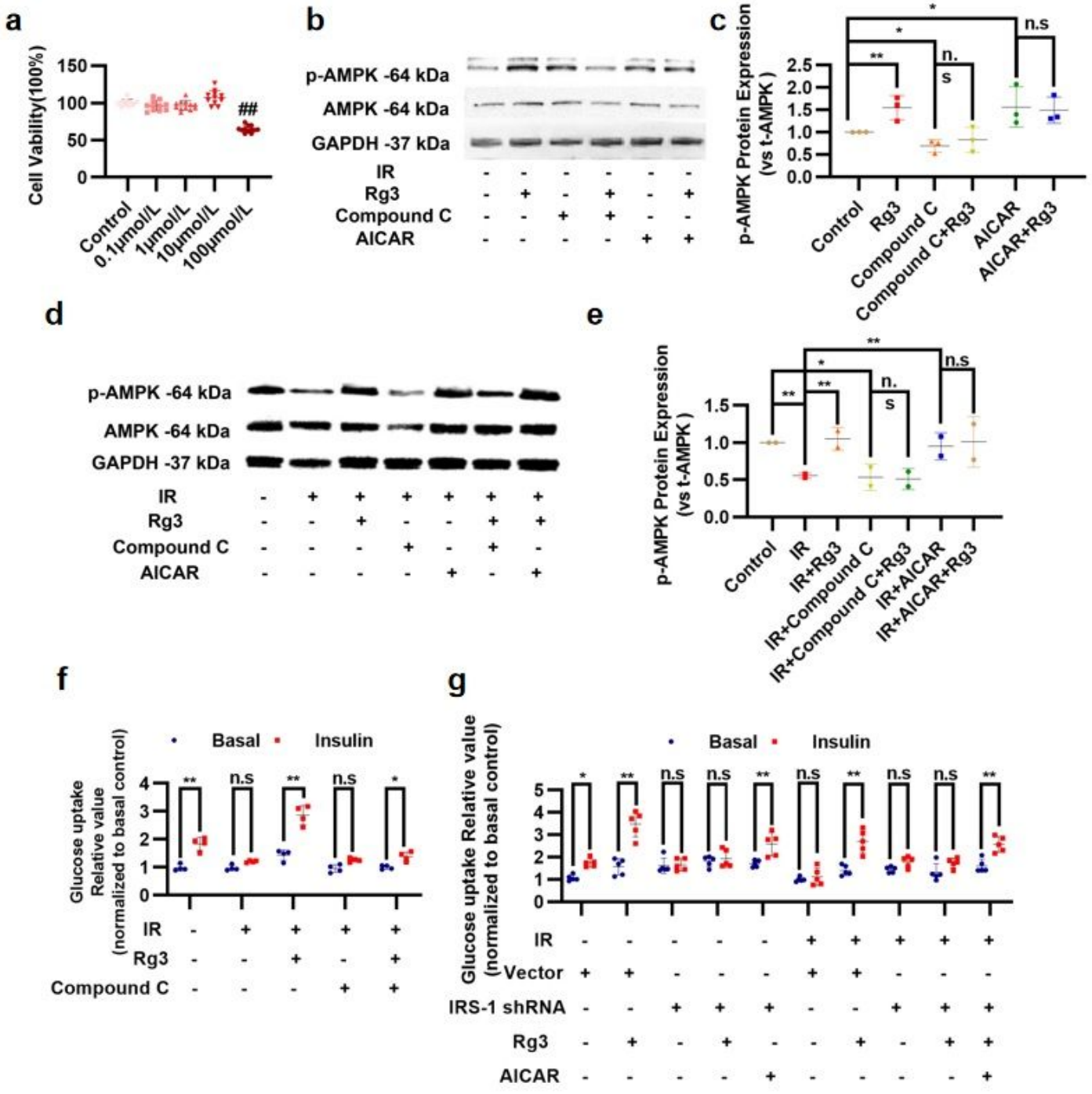


Figure 7

The effect of ginsenoside Rg3 on the promotion of glucose uptake in IR-H9c2 cells by AMPK activation was dependent on the insulin signaling pathway. (a) The cell viability was detected by MTT assay(n 10-12 each group). (b) Representative Western immunoblots for p-AMPK and t-AMPK in normal H9c2 cells(n 3 each group). (c) Bar graph showing corresponding quantitative data for Western blotting(n 3 each group). (d) Representative Western immunoblots for p-AMPK and t-AMPK in IR-H9c2 cardiomyocytes(n 3 each group). (e) Bar graph showing corresponding quantitative data for Western blotting(n 3 each group). (f-g) Glucose uptake in IR-H9c2 cardiomyocytes was evaluated using 2-NBDG fluorescent probes(844 n 3 each group).

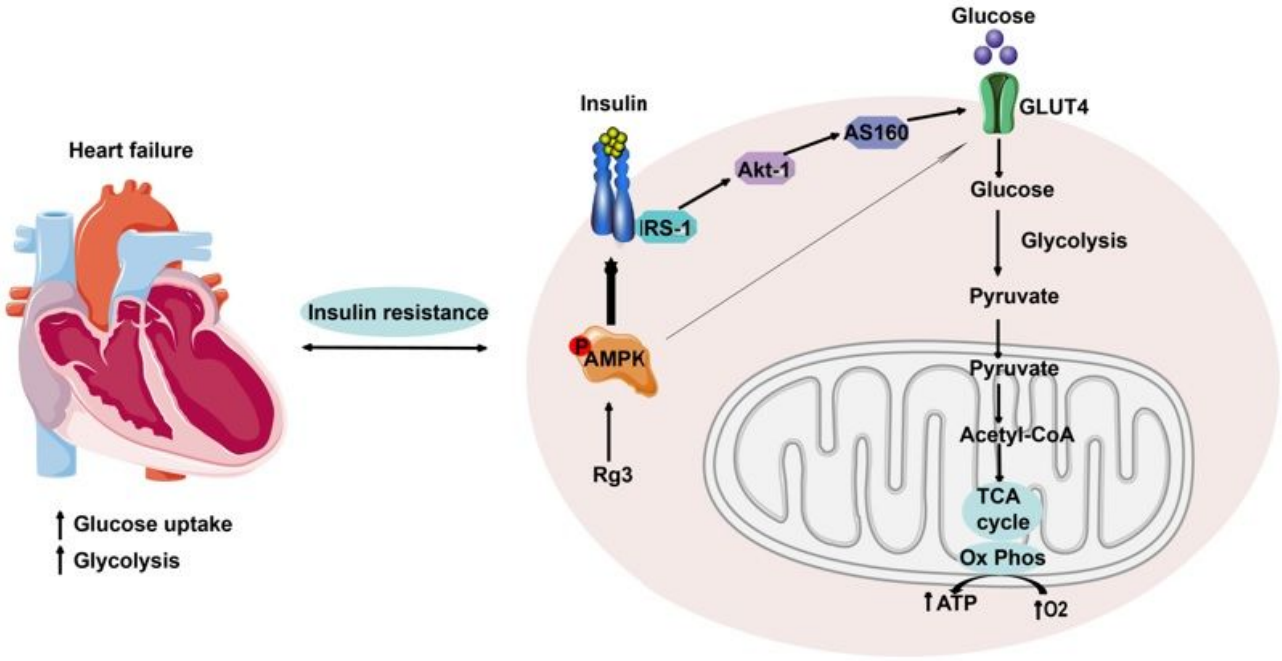


**Figure 8**

(caption not included)

## Supplementary Files

This is a list of supplementary files associated with this preprint. Click to download.

- FigureS1.jpg